Exonuclease action of replicative polymerase gamma drives damage-induced mitochondrial DNA clearance

Akshaya Seshadri[1,2] and Anjana Badrinarayanan[1*]

[1]National Centre for Biological Sciences-TIFR, Bangalore; [2]SASTRA University, Thanjavur

Correspondence to: anjana@ncbs.res.in

Keywords: mitochondria, mtDNA damage, PolG, Mip1, DNA replication, proof-reading, *S. cerevisiae*

Abstract

Mitochondrial DNA (mtDNA) replication is essential for mitochondrial function. This is carried out by a dedicated DNA polymerase gamma, with 5'-3' polymerase and 3'-5' proofreading/ exonuclease activity. Perturbations to either properties can have pathological consequences. Predominant sources for replication stress are DNA lesions, such as those induced by oxidative damage. How mtDNA lesions affect the polymerase activity and mtDNA stability *in vivo* is not fully understood. To address this, we induce mtDNA-specific damage in *S. cerevisiae.* We observe that mtDNA damage results in significant mtDNA loss. This loss occurs independent of cell cycle progression or cell division, suggesting an active mechanism for damaged mtDNA clearance. We implicate the 3'-5' exonuclease activity of the mtDNA polymerase in this clearance, with rates of loss being affected by cellular dNTP levels. We propose a model where polymerase encounter with DNA lesions transitions its activity from synthesis to degradation, resulting in damaged mtDNA clearance. Overall, our findings reveal context-dependent, selective regulation of two critical but opposing functions of polymerase gamma to ensure mitochondrial genome integrity.

Introduction

Faithful replication and maintenance of mitochondrial DNA (mtDNA) is essential for mitochondrial function and cell survival. Most eukaryotic cells contain multiple copies of their mtDNA, packaged into distinct mtDNA nucleoids [1]. The number of nucleoids increases as a function of cell volume [2]. Replication of mtDNA within these nucleoids occurs independently of nuclear genome replication [3], [4], and is carried out by a dedicated DNA polymerase, Polymerase gamma (PolG) [5], [6], [7]. PolG belongs to the A-family of polymerases, which includes E. coli DnaI and the T7 DNA polymerase [8]. In metazoans, PolG is a trimeric holoenzyme: a PolGα subunit with 5'-3' polymerase (pol) and 3'-5' exonuclease (exo) domains, and a dimeric PolGβ that increases the processivity of PolGα, via regulation of both pol and exo activity [9]. The budding yeast ortholog of PolG (Mip1) is a processive enzyme encoding the 5'-3' pol and 3'-5' exo domains in a single polypeptide [10]. *In vitro,* PolG (without exonuclease activity) displays an error frequency of $15x10^{-6}$ per nucleotide [11]. The synthesis-associated error rate is reduced to $<8x10^{-6}$ per nucleotide by the exo domain, that recognizes mispaired 3' termini during synthesis [12], [13]. *In vivo,* mutations in exo function can increase mtDNA mutation rates by several 100-fold [14] and mice models of exo-deficient PolG have displayed elevated mtDNA mutations, cardiomyopathy and premature ageing [7].

In addition to maintaining replication fidelity at the site of DNA synthesis, the exonuclease domain of the mitochondrial polymerase plays important roles in other contexts as well. Given the polyploid nature of mtDNA, mutant DNA molecules typically constitute only a small fraction of the total mtDNA. It has been suggested that elimination of the damaged mtDNA copies, combined with the replication of the intact ones could be a mechanism by which mtDNA integrity and function in maintained [15]. In several instances, the exo domain has been implicated in such clearance. For example, linear mtDNA fragments (generated by action of restriction endonucleases) are subject to degradation by the exo domain of PolG [16], [17]. Furthermore, in conditions of extreme starvation in yeast, it has been shown that exonuclease domain of Mip1 results in mtDNA clearance, likely as a salvage pathway to replenish dNTP levels [18]. Interestingly, in Trypanosoma, one of the six mtDNA polymerases was recently shown to function as an exonuclease only, as it lacked the catalytic activities associated with pol function [19].

It remains unclear as to how the exonucleolytic function, that is typically restricted to only a few bases around the terminal nucleotides in a primer strand, is extended to these different capacities, while still maintaining of balance between pol and exo activity. Indeed, imbalance in the same can have direct consequences on replication fidelity as well as total amount of DNA synthesis carried out by the polymerase [20]. Even within the context of mtDNA replication, the polymerase is likely to encounter replication-stalling lesions, such as those generated by oxidative damage, frequently during DNA synthesis, in part due to the reactive oxygen species rich environment mtDNA resides in [21]. This makes mtDNA susceptible to damage significantly more than its nuclear counterpart [22], with point mutation rates of mtDNA reported to be ~10-fold higher than the nuclear genome [23], [24]. How the polymerase responds to such DNA lesions *in vivo,* and how pol/ exo balance is maintained to ensure mtDNA integrity in such a scenario remains unknown.

We had previously developed a tool to induce mtDNA-specific damage. For this, we mitochondrially-targeted the bacterial toxin, DarT (mtDarT), which generates adducts on single-stranded DNA, to induce replication-stalling lesions specifically on mtDNA [25], [26], [27]. In this study, we utilized mtDarT to understand how such lesions affect mtDNA maintenance and PolG (Mip1 henceforth) function *in vivo* in *S. cerevisiae.* We specifically monitored the impact of mtDNA damage mediated by these lesions on mtDNA copy number. We found that mtDNA damage resulted in mtDNA loss. This loss was independent of cell cycle progression or cell division, suggesting an active mechanism of mtDNA clearance. In support, we uncovered a role for the 3'-5' exonuclease of Mip1 in this mtDNA loss under damage, with cellular dNTP levels regulating the rates of clearance. Our results are consistent with a model where Mip1 encounter with a DNA lesion switches its function from synthesis to degradative, thus resulting in the clearance of lesion-containing mtDNA. Together, our work highlights the selective regulation of pol/exo balance for the maintenance of mtDNA integrity under DNA damage.

Results

mtDNA damage results in mtDNA loss

To study the effect of mtDNA damage on mtDNA maintenance, we utilized a tool that was previously characterised by our group to specifically damage mtDNA in *S. cerevisiae* [27]. For this, we expressed mitochondrially-targeted DarT (mtDarT) from a β-estradiol-inducible promoter in yeast cells [27] (Fig. S1A). We first confirmed expression of mtDarT via Western

blotting and found robust induction of mtDarT 4 and 8 hrs after addition of β-estradiol (Fig. S1B). Furthermore, cells expressing mtDarT were compromised in survival, as assessed by their growth on plates carrying β-estradiol. This was in contrast to empty vector control cells, which did not show a growth defect on β-estradiol containing plates (Fig. S1C). We then proceeded to monitor the fate of mtDNA in cells subjected to damage via SYBR Green I (SGI) staining in live cells [28]. As a control, we compared mtDarT-expressing cells with cells carrying an empty vector and subjected to the same experimental regime (Fig. S1A).

In the absence of damage, pulse-staining with SGI resulted in the labelling of mtDNA nucleoids [28], that were seen as distinct cytoplasmic puncta in the cell (Fig. 1A). These puncta were localized in the mitochondria (Fig. S1D), and no nuclear DNA staining was observed (Fig. S1D). As a control, SGI staining of ρ^0 cells (with lack mtDNA) resulted in nuclear DNA staining and no cytoplasmic puncta were observed (Fig. S1E). In the absence of damage, multiple mtDNA foci were observed in all cells (ρ^+) (Fig. 1A). We found that the number of mtDNA foci per cell increased as a function of cell area, in line with previous observations showing mtDNA scaling with increasing cell size [2] (empty vector (0 hr), Spearman's correlation coefficient ($\boldsymbol{\rho}$) 0.76, CI: 12.43503, 13.18894) (Fig. 1B). The percentage of ρ^+ cells as well as the relationship of the number of nucleoids with cell area was maintained in empty vector cells, even after 4 and 8 hrs of β-estradiol treatment (Fig. 1B-C).

Upon induction of mtDarT, we observed fewer mtDNA nucleoids per cell, when compared to the empty vector control (Fig 1A, mtDarT). At 8 hrs post-induction, the relationship between number of mtDNA nucleoids and cell area was significantly perturbed (Spearman's correlation coefficient ($\boldsymbol{\rho}$) 0.53, CI: 8.851388, 9.779604) (Fig. 1B), and the percentage of ρ^0 cells increased gradually, with 32±4% ρ^0 cells observed after 8 hrs of mtDarT induction (Fig. 1C). Indeed, majority of cells had fewer than 10 mtDNA nucleoids per cell 8 hrs after damage induction (Fig. 1D). Consistent with the depletion of mtDNA in these conditions, we found that mtDarT-expressing cells frequently displayed nuclear DNA staining as well (Fig. 1A). This mtDNA loss was not accompanied by reduction in mitochondrial content, as assessed by the levels of the Cox4 protein (Fig. S1F). Together, these observations suggest that mtDNA damage results in mtDNA loss.

mtDNA loss occurs independent of cell cycle progression

What cellular mechanisms might result in the observed loss of mtDNA? We first considered the possibility that asymmetric partitioning of damaged mtDNA during division could result in the generation of ρ^0 cells [29]. In this scenario, cells at each division would receive fewer

118 numbers of mtDNA nucleoids (or no nucleoids at all). To test this possibility, we arrested cells
119 in either G1/S or G2/M and then induced mtDarT to follow the fate of mtDNA under damage
120 in non-dividing cells.

121 For this, we first pre-treated Δ*bar1* cells (*MAT***a**) with α-factor which resulted in a G1/S phase
122 arrest (Fig. 2A), following which we induced mtDNA damage in this arrested population. We
123 observed that mtDNA nucleoid staining was reduced in arrested cells after 8 hrs of damage,
124 with few to no mtDNA nucleoids in these highly elongated cells (Fig. 2B). Similarly, the
125 relationship between cell size and number of mtDNA nucleoids was also perturbed in the
126 arrested cells expressing mtDarT (***ρ*** = 0.44 (CI: 12.65272, 15.20398) (Fig. 2F). In contrast,
127 empty vector cells had densely packed mtDNA nucleoid foci dispersed throughout the cell (Fig.
128 2B) and the relationship between cell size and number of mtDNA nucleoids was also
129 maintained (***ρ*** = 0.87 (CI: 33.81381, 40.35107) (Fig. 2F). Thus, G1/S arrested cells showed
130 mtDNA loss under damage (Fig. 2C-D,). To eliminate any potential influence from the cell
131 cycle stage under arrest, we separately investigated mtDNA loss in nocodazole-induced G2/M-
132 arrested cells (Fig. S2A). Upon mtDarT expression, here too we observed a decrease in
133 frequency of ρ^+ cells in G2/M arrest (Fig. S2B), similar to that observed in G1/S arrested cells.
134 Taken together, these observations indicate that cell cycle progression (and cell division) does
135 not contribute to mtDNA loss under mtDNA damage.

136 **mtDNA loss is dependent on the exonuclease activity of Mip1**

137 Since mtDNA loss in response to mtDNA damage occurred even in non-dividing cells, we
138 considered the possibility of an active mtDNA clearance mechanism, such as nuclease-
139 mediated DNA degradation under damage. In *S. cerevisiae,* Nuc1, homolog to the mammalian
140 EndoG, is the major mitochondrial endonuclease [30]. In order to check if Nuc1 was
141 responsible for clearing out mtDNA under damage, we deleted Nuc1 and tested the effect of
142 the same on mtDNA nucleoid numbers. We observed that Nuc1 was not essential for mtDNA
143 loss under damage (Fig. S3A-B). Instead, we found that mtDNA loss was exacerbated in cells
144 lacking *nuc1*. It is possible that Nuc1 contributes to mtDNA damage repair in these conditions,
145 and that another nuclease may be driving mtDNA clearance under damage.

146 Another nuclease that has been connected with mtDNA clearance is the exonuclease domain
147 of the mitochondrial replicative polymerase (PolG/ Mip1). In mammalian cells, PolG
148 exonuclease domain contributes to degradation of linear mtDNA fragments [16], [17].

149 Similarly, in yeast cells facing extreme starvation, the exo domain of Mip1 has been implicated
150 in mtDNA clearance [18]. Whether such activity is also relevant in the context of mtDNA
151 damage is unknown. We thus assessed whether the exonuclease activity of Mip1 in under
152 conditions of DNA damage could also result in mtDNA degradation.

153 Based on previously characterized mutations, we generated an exonuclease-deficient Mip1 via
154 mutating 2 catalytic residues in the ExoI motif of the enzyme, Asp171 to Ala171 and Glu173
155 to Ala173 (*mip1*$^{exo-}$ henceforth) [12], [18], [31] (Fig. 3A). Mip1 and *mip1*$^{exo-}$ were expressed
156 from their endogenous locus on the chromosome. Western blot experiments confirmed that
157 their expression in empty vector and mtDarT-induced samples were comparable (Fig. S3C).
158 We did note that *mip1*$^{exo-}$ cells expressing mtDarT showed an elevated level of ρ^0 cells prior to
159 damage induction (Fig. 3C-D). However, upon mtDarT induction, *mip1*$^{exo-}$ cells maintained
160 mtDNA nucleoids even after 8 hrs of damage, and no damage-induced mtDNA depletion was
161 observed (Fig. 3C-D). Although there was no loss of mtDNA, the relationship between number
162 of mtDNA nucleoids and cell area was still perturbed in this background (Spearman's
163 correlation coefficient (***ρ***) 0.44, CI: 13.54795, 14.56954) (Fig. 3E, mtDarT). These
164 observations suggest that the exonuclease activity of the mitochondrial replicative polymerase
165 drives mtDNA loss under DNA damage. The compromised scaling of mtDNA nucleoid
166 numbers with increasing cell size even in the absence of exo suggests that replication
167 progression could be additionally compromised under mtDNA damage.

168 **mtDNA loss is dependent on the polymerase and exonuclease domains of Mip1**

169 To confirm that exonuclease activity is indeed directly driving mtDNA clearance under
170 damage, we complemented the *mip1*$^{exo-}$ construct with ectopic expression of the exo domain in
171 this background. For this, we generated two variants of *mip1* expressed from the Mip1
172 promoter on a low copy replicating plasmid (Fig. 4): A. Mip1-CΔ669 where the entire pol
173 domain is absent, but encompasses intact exo domain with the linker region. And B. Mip1-
174 CΔ263 where the last 263 amino acids in the C-terminus of Mip1 are deleted. This construct is
175 deficient in polymerization activity, but still retains the ability of pol to bind DNA, as well as
176 an intact exo domain [32], [33]. We confirmed the expression of the truncated proteins via
177 Western blot and that both constructs colocalized with mitochondrial nucleoids (Fig. S4A-B).

178 We first expressed Mip1-CΔ669 in *mip1*$^{exo-}$ cells under mtDNA damage and followed the fate
179 of mtDNA nucleoids in these conditions. After 8 hrs of damage, the percentage of ρ^+ cells and

180 the distribution of number of nucleoids per cell did not change significantly in cells expressing
181 Mip1-CΔ669 (Fig. 4A-C). Thus, expression of the exonuclease domain alone was insufficient
182 to fully complement exo function under damage. In contrast, cells expressing Mip1-CΔ263 in
183 *mip1*$^{exo-}$ background showed a significant decrease in frequency of ρ^+ cells upon mtDNA
184 damage induction (Fig. 4D-E). This was additionally supported by reduction in the number of
185 mtDNA nucleoids per cell in *mip1*$^{exo-}$ cells expressing Mip1-CΔ263 under damage (Fig. 4F).
186 Together, these results support a direct role for the exonuclease domain of Mip1 in mtDNA
187 clearance under conditions of mtDNA damage.

188 **Rates of mtDNA loss are influenced by dNTP levels**

189 Our above observations imply that the polymerase domain (but not activity) is required for the
190 exonuclease domain to access DNA for degradation, as a polymerization-deficient but DNA
191 binding-proficient pol domain (Mip1-CΔ263) was required for exonuclease function. However,
192 Mip1-CΔ669 (lacking the polymerase domain completely) failed to induce mtDNA clearance
193 in *mip1*$^{exo-}$ cells. Given the need of both polymerase and exonuclease domains for mtDNA
194 clearance under damage, it is possible that exo-mediated clearance occurred on mtDNA that is
195 being actively replicated by Mip1. We thus hypothesized that increasing polymerase activity
196 (and hence access) on mtDNA should impact the rates of mtDNA loss under damage. Studies
197 in *S. cerevisiae* have shown that elevation in dNTP levels can increase Mip1 polymerase
198 function [18], [34], [35], [36]. We hence deleted Sml1, a negative regulator of ribonucleotide
199 reductase (RNR) activity in *S. cerevisiae,* that results in an increase in cellular dNTP levels
200 [37], and assessed the rates of mtDNA clearance under damage in this background.

201 We confirmed the Mip1 expression was not perturbed the Δ*sml1* background (Fig. S5A).
202 Furthermore, Δ*sml1* cells grew similarly to wild type cells (Fig. S5B), and had comparable
203 number of mtDNA nucleoids in the absence of damage (Fig. 5A). In contrast, upon mtDarT
204 induction, Δ*sml1* cells showed a significant increase in mtDNA loss. In comparison to wild
205 type, the rates of mtDNA loss were higher in Δ*sml1* cells, as demonstrated by faster reduction
206 in the number of mtDNA nucleoids per cell and increase in the proportion of ρ^0 cells within 4
207 hrs of mtDarT induction (Fig. 5B-C). At 8 hrs after damage induction, percentage of ρ^0 cells
208 was found to be 55±5% and 32±4% in Δ*sml1* and wild type cells respectively. Importantly, this
209 elevated mtDNA loss in Δ*sml1* cells was dependent on the exonuclease activity of Mip1, with
210 no loss being observed in Δ*sml1 mip1*$^{exo-}$ cells (Fig. S5C-D).

211 In sum, our observations implicate the exonuclease domain of Mip1 in mtDNA clearance under
212 conditions of mtDNA damage. Our results are consistent with a scenario where increased
213 access of Mip1 to mtDNA (for example, via elevated dNTP levels) may increase the chance of
214 Mip1 encountering DNA lesions and thus result in further mtDNA degradation by exo.

215 Discussion

216 Taken together, our study places the exonuclease activity of PolG as a central mediator of mtDNA loss
217 under mtDNA damage conditions. Thus, the clearance of dysfunctional mtDNA copies employs
218 the very apparatus that replicates it. Such a mechanism of damaged mtDNA clearance would
219 restrict the degradative function of the polymerase to the damaged mtDNA alone, and
220 circumvent the requirement to have an additional pathway to sense and respond to the damage
221 more globally. Indeed, such drastic DNA loss might only be tolerated in a multicopy genome,
222 allowing cells to lose most copies yet retain the capacity to restore homeostasis post-damage
223 removal, in line with the 'disposable genome' hypothesis for mitochondria [15].
224 How are contrasting functions of Mip1 polymerase and exonuclease selectively regulated in
225 this context-dependent manner (replication vs degradation)? A recent structural analysis of
226 PolG showed that proofreading is carried out in the pol domain itself [38]. Upon detecting a
227 mismatch synthesis is halted, the mismatched primer is removed from the finger domain and
228 shuttled to the exo domain for degradation. Thus, the exo site likely degrades any DNA shuttled
229 to it, irrespective of whether there is a mismatch or not [39]. This is consistent with other reports
230 that suggest that exo plays only a passive role in proofreading [40]. While early studies have
231 found that exo mutants can be complemented in trans [41], [42], [43], the final switch of the
232 primer from pol to exo could occur inter-molecularly via dissociation, followed by re-
233 association or intra-molecularly within the originally bound holoenzyme[44], [45], [46]. Our
234 observations suggest that although exo is capable of catalysis exogenously, it is still dependent
235 on a pol domain for access to DNA. We thus propose that the hand-off from synthesis to
236 degradation occurs at the site of replication stalling. Such an arrangement would ensure that
237 the exonucleolytic action of Mip1 is regulated to prevent promiscuous mtDNA clearance in the
238 absence of DNA damage. How much DNA is degraded by a single exonuclease under damage
239 conditions, the rates of degradation and the dynamics of mtDNA resynthesis upon removal of
240 the stress are exciting and outstanding questions.
241 In our proposed model, mtDNA clearance would be restricted to the damaged genome alone.
242 In the context of heteroplasmy [47], where only a fraction of mtDNA would typically carry a
243 mutation, this selective clearance would allow the retention of intact genomes over the mutant

244 copies. In support, studies in drosophila cells have shown preferential replication of non-
245 mutated mtDNA copies [48]. More recently, reports in budding yeast have also shown that
246 mutant mtDNA are compartmentalized via modulation of the cristae morphology [49]. It is
247 possible that exonuclease activity of Mip1 on these sequestered mtDNA would additionally
248 contribute to the selective clearance of damaged genomes.
249 Exonuclease activity of the replicative polymerase is canonically considered in the context of
250 proofreading, where only few mismatched nucleotides from newly synthesized DNA are
251 removed [50]. More recent evidences suggest that the exonuclease domain of the mitochondrial
252 replicative polymerase may play more versatile roles. Exo action has previously been observed
253 on linear mtDNA fragments and under conditions of extreme starvation (when dNTP levels are
254 depleted) [18]. Such DNA degradation has also been reported in the context of the T4 DNA
255 polymerase [51]. Exonuclease activity is also required for mtDNA ligation during replication
256 [52], absence of which results in accumulation of mtDNA fragments. The current implication
257 of exo function in mtDNA clearance under conditions of mtDNA damage suggests that it is a
258 central player in the maintenance of mtDNA integrity as well, beyond the regulation of
259 replication-associated errors. Indeed, the choice to repair or degrade damaged mtDNA could
260 be driven by the type and quantity of damage. For example, given the absence of active
261 nucleotide excision repair in mitochondria [53][54], it is possible that the exo-mediated
262 pathway for mtDNA degradation may be the first response to persistent, replication-stalling
263 lesions. Other contexts can include mtDNA deletions or mutations, where selective degradation
264 of the damaged copies would be a reliable mechanism for ensuring mitochondrial genome
265 integrity maintenance.
266
267

268 ## Materials and methods:

269 **Yeast strains, media and growth conditions**

270 Strains, plasmids and oligos used in this study are listed in tables S1, S2 and S3 respectively.
271 Cells were grown at 30ºC with 180rpm shaking, in YP (yeast extract 1%, peptone 2%) medium.
272 Experiments were performed in non-fermentable conditions using glycerol (2%) as the carbon
273 source. Dextrose (2%, fermentable medium) was used for preparatory experiments including
274 transformations etc. All experiments were performed in log-phase of growth (0D600, between
275 0.2-0.4). Appropriate antibiotics and inducers were added to the medium as required. All strains
276 generated were haploid prototrophs belonging to CEN.PK background [55]. For generating
277 strains with C-terminal tagging or deletion of a genomic locus, PCR-based targeted
278 homologous recombination strategy was used as described in [56]. All strains were verified by
279 PCR's followed by fluorescence microscopy and/or western blotting for validating the insertion
280 of epitope tags. The details of strains and plasmids construction are provided in tables S1 and
281 S2 respectively.
282 Plasmids for expression of the empty vector (NABC557), mtDarT (NABC561), Mip1-Δ669
283 (NABC776) and Mip1-Δ263 (NABC775) were freshly transformed into yeast cells before
284 experiments. This was to prevent mtDNA instability that might arise from the continuous
285 maintenance and expression of both the toxin and Mip1 truncations. Below, we provide the
286 strategy used to generate the Mip1 mutations.
287

288 **mtDNA damage induction**

289 The protocol for inducing mtDNA damage was adopted from [27]. Briefly, cells carrying empty
290 vector control plasmid (NABC557) or mtDarT plasmid (NABC561), carrying NAT resistance,
291 were transformed into yeast cell cells using the standard Lithium acetate protocol.
292 Transformants carrying the plasmid were selected by plating on media containing
293 Nourseothricin (NTC). Colonies were subsequently inoculated in YPG cultures containing
294 NTC for plasmid maintenance. Upon reaching early log-phase (OD~0.2-0.4), samples were
295 collected (0 hr). Subsequently, the cultures were treated with 100nM β-estradiol (Sigma) to
296 induce expression. Inducer was maintained at all the times during the experiment (persistent
297 damage). Samples were collected at various intervals (4, 8 hrs post-induction) as indicated for
298 specific experiments.
299

300 **Survival assay**

301 Survival assay to compare growth between different strains was performed by serially diluting
302 log phase cultures (OD600 of 0.06, diluted 10x, until $6x10^{-9}$). 6µl of the diluted culture was
303 spotted on agar plates with respective selection markers. The plates were incubated at 30ºC,
304 and growth was monitored.
305
306 **Live cell staining of mt-nucleoids**
307 Mt-nucleoids were stained in live cells using SYBR Green I (Invitrogen, S7563). The protocol
308 was adopted from [28]. In brief, 1 ml aliquots of cultures were taken at specified time points,
309 pelleted and washed in 1X PBS. This was followed by resuspension of cells in 1X PBS
310 followed by addition of 0.5ul of 10,000X SYBR Green I. After gently mixing the contents, the
311 mixture was immediately spun down and washed with 1X PBS. The pellet was resuspended in
312 appropriated volume of 1X PBS. 1µl of diluted culture was spotted on 1% water agarose pads
313 (Invitrogen, 16500500) for microscopy.
314 For DAPI staining, 1ml cultures were spun down and the pellets were resuspended in 1X PBS.
315 0.5ul of 10mg/ml DAPI. The dye was resuspended gently into the cell pellet and the mixture
316 was immediately spun down. The pellet was washed with 1X PBS, twice, before resuspending
317 it in appropriate volume of 1X PBS. 1µl of diluted culture was spotted on 1% water agarose
318 pads for microscopy.
319
320 **Western blot**
321 Trichloroacetic acid (TCA) extraction method, as previously described, was used [27]. Dilution
322 and details of the antibodies can be found in Table S4. The protein bands were detected using
323 chemiluminescence substrate based assay (Supersignal West PICO or FEMTO PLUS).
324 Separately, in each case a second protein gel was probed as loading control, and visualized with
325 Coomassie brilliant blue staining solution. For quantification of relative proteins levels, band
326 intensities of protein of interest were obtained from ImageJ. Values were normalized to the
327 intensity of the loading control.
328
329 **G1/S arrest using α-factor**
330 To arrest yeast cells in G1/S phase using α-factor (mating pheromone), Δ*bar1* (*MAT***a**) strain
331 was used. Overnight cultures of cells expressing empty vector or mtDarT were grown to
332 appropriate OD (early log phase, 0.2-0.6), after which they were pelleted. The cell pellet was
333 carefully resuspended in a pre-warmed YPG medium containing α-factor (final concentration
334 of 25ng/ml, from 10µg/ml stock solution in Methanol) and NAT. The culture was placed in an

335 incubator for 3 hours for arrest to occur completely. After 3 hours, majority of cells were
336 arrested in G1/S phase as revealed by the formation of schmoo cells with oblong morphology
337 [57]. Upon reaching this stage, inducer (β-estradiol) was added and samples were collected to
338 monitor the mt-nucleoid status. To maintain continuous arrest, cells were pelleted and
339 resuspended in media containing fresh α-factor every 3 hours.
340
341 **G2/M arrest using Nocodazole**
342 Overnight cultures of cells expressing empty vector or mtDarT were grown to appropriate OD
343 (early log phase, 0.2-0.6), after which they were pelleted. The cell pellet was carefully
344 resuspended in pre-warmed YPG medium containing Nocodazole (final concentration of
345 9µl/ml, from 1.5mg/ml stock solution) and NAT. The culture was placed in an incubator for 3
346 hours for arrest to occur completely. After 3 hours, majority of cells were arrested in G2/M
347 phase as revealed by the dumbbell shape of these cells [57]. Upon reaching this stage, inducer
348 (β-estradiol) was added and samples were collected to monitor the mt-nucleoid status. To
349 maintain continuous arrest, cells were pelleted and resuspended in media containing fresh
350 Nocodazole every 3 hours.
351
352 **Flow cytometry**
353 Cell cycle analysis using flow cytometry was performed following the protocol from [58].
354 Cultures were collected and centrifuged at 3000 rpm, for 3 mins at room temperature. After
355 discarding the media, the cells were fixed in 70% ethanol overnight at 40ºC. Following fixation,
356 cells were pelleted and subsequently washed in 1ml of 50 mM Sodium citrate (pH 7.5). Cells
357 were then re-suspended in 500µl RNAse A buffer (500ul sodium citrate buffer + 5µl RNase A)
358 and incubated with shaking at 50ºC for 2 hours with shaking (350 rpm). Cells were then pelleted
359 and re-suspended in Proteinase K solution (20ul enzyme (2mg/ml) + 180µl sodium citrate
360 buffer). They were then incubated at 37ºC for 1 hr, with shaking (350 rpm). Following
361 Proteinase K treatment, cells were pelleted, washed and re-suspended in 1ml of sodium citrate
362 buffer. 100µl of this sample was made upto 1.0ml with sodium citrate buffer containing 1µM
363 SYTOX Green. The sample was sonicated on ice, at 20% amplitude for 10 secs with two 5 secs
364 pulses with a gap of 5 secs. Flow cytometry analysis was performed on Accuri C6+ flow
365 cytometer.
366
367 **Fluorescence microscopy and image analysis**

368 Fluorescence imaging of budding yeast cells were carried out on a wide-field, epifluorescence
369 microscope (Nikon Eclipse Ti2-E), with motorized XY-stage, 60X plan apochromat objective
370 (NA 1.41) and a pE4000 light source (CoolLED). Focus was maintained using an infrared-
371 based Perfect focus system. Z scanning was done using motorized Z-control. Z-stacks were
372 acquired across 7µm of the cell in steps of 0.3µm. Images were acquired with Hamamatsu Orca
373 Flash 4.0 camera using NIS-elements software (version 5.01).
374 Image analysis
375 Following acquisition, image stacks were deconvolved in NIS-elements software using 3D-
376 Lucy-Richardson method. A maximum projection of the deconvolved stacks was generated in
377 ImageJ for fluorescence image analysis. For fluorescence analyses, a maximum projected
378 fluorescence image stack was generated on ImageJ. Total number of nucleoids was obtained
379 using the 3D-maxima finder plugin in ImageJ. Cell segmentation was performed using Cell-
380 ACDC program [59] generating cell ROI's for single cell based analyses. Number of nucleoids
381 per cell was obtained by custom macros written using the Mitochondria analyser plugin [60]
382 in ImageJ where the number of foci was overlayed on cell ROI's to obtain number of nucleoid
383 foci per cell. Cell area was calculated using Analyse Particles function in ImageJ. Correlation
384 density plots were plotted using RStudio (Version 1.3.1093).
385 For colocalization analysis, line profiles were created on composite images using ImageJ to
386 generate intensity values. The values obtained for each channel was overlayed and plotted using
387 GraphPad Prism (8.4.2) software. Quantification of percentage of ρ^+ cells was done using
388 mother cells alone to avoid inconsistencies that might arise from incomplete mtDNA
389 segregation in bud cells. Correlation plots and density plots for mt-nucleoid number scaling
390 per cell were plotted ignoring the zero values for ρ^0 cells. For these plots, all the cells (mother,
391 bud) in the image field were used.
392
393 **Statistical analysis**
394 After assessing normality, parametric t-tests or non-parametric Wilcoxon's test were performed
395 on GraphPad Prism (8.4.2) to compare differences in percentages of ρ^+ cells. Details of the test
396 for each dataset including results obtained can be accessed in Table S5. For assessing
397 correlations, Spearman's correlation coefficient (for data distributions that are not normal) was
398 obtained through custom scripts on R. P values $\leq$ 0.05 were considered to be significant,
399 indicated by "*", P values $\leq$ 0.01 by "**", P values $\leq$ 0.001 by "***" and P values $\leq$ 0.0001 by
400 "****". P values > 0.05 were considered non-significant.

Acknowledgements

The authors are grateful to Dr. Nitish Dua for sharing of reagents. The authors thank Dr. Nitish Dua, Dr. Asha Mary Joseph and Mr. Aditya Kamat for helpful discussions and feedback on the manuscript. The authors would like to thank Dr. Francesco Padovani for assistance with CellACDC customizations. The authors would like to thank Mr. Anton Iyer for help with coding. This work was supported by fellowships from CSIR (AS) as well as grants from HFSP RPG (AB) and intramural funding from NCBS-TIFR (AB).

Author contributions

AS: conception of project, experimental design, generation of tools and reagents, execution of experiments, data analysis, writing of manuscript. AB: conception of project, project supervision, experimental design and writing of manuscript.

Declaration of interests

The authors declare no competing interests.

References

[1] X. J. Chen and R. A. Butow, "The organization and inheritance of the mitochondrial genome," *Nat. Rev. Genet.*, vol. 6, no. 11, pp. 815–825, Nov. 2005, doi: 10.1038/nrg1708.

[2] A. Seel *et al.*, "Regulation with cell size ensures mitochondrial DNA homeostasis during cell growth," *Nat. Struct. Mol. Biol.*, vol. 30, no. 10, pp. 1549–1560, Oct. 2023, doi: 10.1038/S41594-023-01091-8.

[3] D. Bogenhagen and D. A. Clayton, "Mouse L cell mitochondrial DNA molecules are selected randomly for replication throughout the cell cycle," *Cell*, vol. 11, no. 4, pp. 719–727, 1977, doi: 10.1016/0092-8674(77)90286-0.

[4] T. Sasaki, Y. Sato, T. Higashiyama, and N. Sasaki, "Live imaging reveals the dynamics and regulation of mitochondrial nucleoids during the cell cycle in Fucci2-HeLa cells," *Sci. Reports 2017 71*, vol. 7, no. 1, pp. 1–12, Sep. 2017, doi: 10.1038/s41598-017-10843-8.

[5] A. Genga, L. Bianchi, and F. Foury, "A nuclear mutant of Saccharomyces cerevisiae deficient in mitochondrial DNA replication and polymerase activity.," *J. Biol. Chem.*, vol. 261, no. 20, pp. 9328–9332, Jul. 1986, doi: 10.1016/S0021-9258(18)67658-6.

[6] P. Lestienne, "Evidence for a direct role of the DNA polymerase gamma in the replication of the human mitochondrial DNA in vitro," *Biochem. Biophys. Res. Commun.*, vol. 146, no. 3, pp. 1146–1153, Aug. 1987, doi: 10.1016/0006-291X(87)90767-4.

[7] W. C. Copeland and M. J. Longley, "Mitochondrial genome maintenance in health and disease," *DNA Repair (Amst).*, vol. 19, pp. 190–198, 2014, doi: 10.1016/J.DNAREP.2014.03.010.

[8] L. S. Kaguni, "DNA Polymerase γ, The Mitochondrial Replicase1," *https://doi.org/10.1146/annurev.biochem.72.121801.161455*, vol. 73, pp. 293–320, Jun. 2004, doi: 10.1146/ANNUREV.BIOCHEM.72.121801.161455.

[9] M. T. Oliveira, J. Haukka, and L. S. Kaguni, "Evolution of the Metazoan Mitochondrial Replicase," *Genome Biol. Evol.*, vol. 7, no. 4, p. 943, Apr. 2015, doi: 10.1093/GBE/EVV042.

[10] K. Viikov, P. Väljamäe, and J. Sedman, "Yeast mitochondrial DNA polymerase is a highly processive single-subunit enzyme," *Mitochondrion*, vol. 11, no. 1, pp. 119–126, Jan. 2011, doi: 10.1016/J.MITO.2010.08.007.

[11] M. J. Longley, D. Nguyen, T. A. Kunkel, and W. C. Copeland, "The Fidelity of Human DNA Polymerase γ with and without Exonucleolytic Proofreading and the p55 Accessory Subunit," *J. Biol. Chem.*, vol. 276, no. 42, pp. 38555–38562, Oct. 2001, doi: 10.1074/JBC.M105230200.

[12] F. Foury and S. Vanderstraeten, “Yeast mitochondrial DNA mutators with deficient proofreading exonucleolytic activity.,” *EMBO J.*, vol. 11, no. 7, pp. 2717–2726, Jul. 1992, doi: 10.1002/J.1460-2075.1992.TB05337.X.

[13] L. S. Kaguni and M. W. Olson, “Mismatch-specific 3’----5’ exonuclease associated with the mitochondrial DNA polymerase from Drosophila embryos.,” *Proc. Natl. Acad. Sci. U. S. A.*, vol. 86, no. 17, p. 6469, 1989, doi: 10.1073/PNAS.86.17.6469.

[14] F. Foury, J. Hu, and S. Vanderstraeten, “Mitochondrial DNA mutators,” *Cell. Mol. Life Sci.*, vol. 61, no. 22, pp. 2799–2811, Nov. 2004, doi: 10.1007/S00018-004-4220-Y/METRICS.

[15] I. N. Shokolenko and M. F. Alexeyev, “Mitochondrial DNA: A disposable genome?,” *Biochimica et Biophysica Acta - Molecular Basis of Disease*, vol. 1852, no. 9. Elsevier, pp. 1805–1809, Sep. 01, 2015. doi: 10.1016/j.bbadis.2015.05.016.

[16] N. Nissanka, S. Bacman, M. Plastini, and C. T. Moraes, “The mitochondrial DNA polymerase gamma degrades linear DNA fragments precluding the formation of deletions,” *Nat. Commun.*, vol. 9, no. 1, Dec. 2018, doi: 10.1038/S41467-018-04895-1.

[17] V. Peeva *et al.*, “Linear mitochondrial DNA is rapidly degraded by components of the replication machinery,” *Nat. Commun.*, vol. 9, no. 1, Dec. 2018, doi: 10.1038/S41467-018-04131-W.

[18] T. C. Medeiros, R. L. Thomas, R. Ghillebert, and M. Graef, “Autophagy balances mtDNA synthesis and degradation by DNA polymerase POLG during starvation,” *J. Cell Biol.*, vol. 217, no. 5, pp. 1601–1611, May 2018, doi: 10.1083/JCB.201801168.

[19] S. B. Delzell, S. W. Nelson, M. P. Frost, and M. M. Klingbeil, “Trypanosoma brucei Mitochondrial DNA Polymerase POLIB Contains a Novel Polymerase Domain Insertion That Confers Dominant Exonuclease Activity,” *Biochemistry*, vol. 61, no. 23, pp. 2751–2765, Dec. 2022, doi: 10.1021/ACS.BIOCHEM.2C00392.

[20] K. Szczepanowska and F. Foury, “A cluster of pathogenic mutations in the 3′–5′ exonuclease domain of DNA polymerase gamma defines a novel module coupling DNA synthesis and degradation,” *Hum. Mol. Genet.*, vol. 19, no. 18, pp. 3516–3529, Sep. 2010, doi: 10.1093/HMG/DDQ267.

[21] A. P. Anderson, X. Luo, W. Russell, and Y. W. Yin, “Oxidative damage diminishes mitochondrial DNA polymerase replication fidelity,” *Nucleic Acids Res.*, vol. 48, no. 2, pp. 817–829, Jan. 2020, doi: 10.1093/NAR/GKZ1018.

[22] F. M. Yakes and B. Van Houten, “Mitochondrial DNA damage is more extensive and persists longer than nuclear DNA damage in human cells following oxidative stress,” *Proc. Natl. Acad. Sci. U. S. A.*, vol. 94, no. 2, p. 514, Jan. 1997, doi: 10.1073/PNAS.94.2.514.

[23] T. J. Parsons *et al.*, “A high observed substitution rate in the human mitochondrial DNA control region,” *Nat. Genet.*, vol. 15, no. 4, pp. 363–368, Apr. 1997, doi:

10.1038/NG0497-363.

[24] C. Haag-Liautard, N. Coffey, D. Houle, M. Lynch, B. Charlesworth, and P. D. Keightley, "Direct Estimation of the Mitochondrial DNA Mutation Rate in Drosophila melanogaster," *PLOS Biol.*, vol. 6, no. 8, p. e204, Aug. 2008, doi: 10.1371/JOURNAL.PBIO.0060204.

[25] G. Jankevicius, A. Ariza, M. Ahel, and I. Ahel, "The Toxin-Antitoxin System DarTG Catalyzes Reversible ADP-Ribosylation of DNA," *Mol. Cell*, vol. 64, no. 6, pp. 1109–1116, Dec. 2016, doi: 10.1016/j.molcel.2016.11.014.

[26] E. Lawarée, G. Jankevicius, C. Cooper, I. Ahel, S. Uphoff, and C. M. Tang, "DNA ADP-Ribosylation Stalls Replication and Is Reversed by RecF-Mediated Homologous Recombination and Nucleotide Excision Repair," *Cell Rep.*, vol. 30, no. 5, pp. 1373-1384.e4, 2020, doi: 10.1016/j.celrep.2020.01.014.

[27] N. Dua, A. Seshadri, and A. Badrinarayanan, "DarT-mediated mtDNA damage induces dynamic reorganization and selective segregation of mitochondria," *J. Cell Biol.*, vol. 221, no. 10, Oct. 2022, doi: 10.1083/JCB.202205104/213451.

[28] R. Jajoo *et al.*, "Accurate concentration control of mitochondria and nucleoids," *Science*, vol. 351, no. 6269, pp. 169–172, Jan. 2016, doi: 10.1126/SCIENCE.AAA8714.

[29] N. Dua and A. Badrinarayanan, "Mechanisms regulating mitochondrial DNA quality control," *J. Transl. Genet. Genomics*, vol. 7, no. 2, pp. 110–125, Jun. 2023, doi: 10.20517/JTGG.2023.08.

[30] P. Dzierzbicki, A. Kaniak-Golik, E. Malc, P. Mieczkowski, and Z. Ciesla, "The generation of oxidative stress-induced rearrangements in Saccharomyces cerevisiae mtDNA is dependent on the Nuc1 (EndoG/ExoG) nuclease and is enhanced by inactivation of the MRX complex," *Mutat. Res.*, vol. 740, no. 1–2, pp. 21–33, Dec. 2012, doi: 10.1016/J.MRFMMM.2012.12.004.

[31] Matthew J. Longley, Philip A. Ropp, and Susan E. Lim, and W. C. Copeland*, "Characterization of the Native and Recombinant Catalytic Subunit of Human DNA Polymerase γ: Identification of Residues Critical for Exonuclease Activity and Dideoxynucleotide Sensitivity," *Biochemistry*, vol. 37, no. 29, pp. 10529–10539, Jul. 1998, doi: 10.1021/BI980772W.

[32] C. H. Trasviña-Arenas *et al.*, "Amino and carboxy-terminal extensions of yeast mitochondrial DNA polymerase assemble both the polymerization and exonuclease active sites," *Mitochondrion*, vol. 49, pp. 166–177, Nov. 2019, doi: 10.1016/J.MITO.2019.08.005.

[33] M. J. Young, R. J. Imperial, S. Lakhi, and D. A. Court, "A non-radioactive DNA synthesis assay demonstrates that elements of the Sigma 1278b Mip1 mitochondrial DNA polymerase domain and C-terminal extension facilitate robust enzyme activity," *Yeast*, vol. 38, no. 4, pp. 262–275, Apr. 2021, doi: 10.1002/YEA.3541.

[34] N. Lecrenier and F. Foury, “Overexpression of the RNR1 gene rescues Saccharomyces cerevisiae mutants in the mitochondrial DNA polymerase-encoding MIP1 gene,” *MGG Mol. Gen. Genet.*, vol. 249, no. 1, pp. 1–7, Jan. 1995, doi: 10.1007/BF00290229/METRICS.

[35] S. Vanderstraeten, S. Van Den Brûle, J. Hu, and F. Foury, “The Role of 3′-5′ Exonucleolytic Proofreading and Mismatch Repair in Yeast Mitochondrial DNA Error Avoidance,” *J. Biol. Chem.*, vol. 273, no. 37, pp. 23690–23697, Sep. 1998, doi: 10.1074/JBC.273.37.23690.

[36] K. Viikov, O. Jasnovidova, T. Tamm, and J. Sedman, “C-Terminal Extension of the Yeast Mitochondrial DNA Polymerase Determines the Balance between Synthesis and Degradation,” *PLoS One*, vol. 7, no. 3, p. e33482, Mar. 2012, doi: 10.1371/JOURNAL.PONE.0033482.

[37] X. Zhao, E. G. D. Muller, and R. Rothstein, “A Suppressor of Two Essential Checkpoint Genes Identifies a Novel Protein that Negatively Affects dNTP Pools,” *Mol. Cell*, vol. 2, no. 3, pp. 329–340, Sep. 1998, doi: 10.1016/S1097-2765(00)80277-4.

[38] J. Park, G. K. Herrmann, P. G. Mitchell, M. B. Sherman, and Y. W. Yin, “Polγ coordinates DNA synthesis and proofreading to ensure mitochondrial genome integrity,” *Nat. Struct. Mol. Biol. 2023 306*, vol. 30, no. 6, pp. 812–823, May 2023, doi: 10.1038/s41594-023-00980-2.

[39] A. Singh, M. Pandey, D. Nandakumar, K. D. Raney, Y. W. Yin, and S. S. Patel, “Excessive excision of correct nucleotides during DNA synthesis explained by replication hurdles,” *EMBO J.*, vol. 39, no. 6, Mar. 2020, doi: 10.15252/EMBJ.2019103367.

[40] R. Fernandez-Leiro, J. Conrad, J. C. Yang, S. M. V. Freund, S. H. W. Scheres, and M. H. Lamers, “Self-correcting mismatches during high-fidelity DNA replication,” *Nat. Struct. Mol. Biol. 2017 242*, vol. 24, no. 2, pp. 140–143, Jan. 2017, doi: 10.1038/nsmb.3348.

[41] E. Baruffini, I. Ferrero, and F. Foury, “Mitochondrial DNA defects in Saccharomyces cerevisiae caused by functional interactions between DNA polymerase gamma mutations associated with disease in human,” *Biochim. Biophys. Acta - Mol. Basis Dis.*, vol. 1772, no. 11–12, pp. 1225–1235, Dec. 2007, doi: 10.1016/J.BBADIS.2007.10.002.

[42] J. D. Stumpf, C. M. Bailey, D. Spell, M. Stillwagon, K. S. Anderson, and W. C. Copeland, “mip1 containing mutations associated with mitochondrial disease causes mutagenesis and depletion of mtDNA in Saccharomyces cerevisiae,” *Hum. Mol. Genet.*, vol. 19, no. 11, p. 2123, Jun. 2010, doi: 10.1093/HMG/DDQ089.

[43] A. Bratic *et al.*, “Complementation between polymerase- and exonuclease-deficient mitochondrial DNA polymerase mutants in genomically engineered flies,” *Nat. Commun.*, vol. 6, Nov. 2015, doi: 10.1038/NCOMMS9808.

[44] C. M. Joyce, "How DNA Travels between the Separate Polymerase and 3′-5′-Exonuclease Sites of DNA Polymerase I (Klenow Fragment)," *J. Biol. Chem.*, vol. 264, no. 18, pp. 10858–10866, Jun. 1989, doi: 10.1016/S0021-9258(18)81699-4.

[45] A. A. Johnson and K. A. Johnson, "Exonuclease Proofreading by Human Mitochondrial DNA Polymerase," *J. Biol. Chem.*, vol. 276, no. 41, pp. 38097–38107, Oct. 2001, doi: 10.1074/JBC.M106046200.

[46] M. W. Olson and L. S. Kaguni, "3′-5′ Exonuclease in Drosophila mitochondrial DNA polymerase: Substrate specificity and functional coordination of nucleotide polymerization and mispair hydrolysis," *J. Biol. Chem.*, vol. 267, no. 32, pp. 23136–23142, Nov. 1992, doi: 10.1016/s0021-9258(18)50067-3.

[47] N. Nissanka and C. T. Moraes, "Mitochondrial DNA heteroplasmy in disease and targeted nuclease-based therapeutic approaches," *EMBO Rep.*, vol. 21, no. 3, Mar. 2020, doi: 10.15252/EMBR.201949612.

[48] J. H. Hill, Z. Chen, and H. Xu, "Selective propagation of functional mitochondrial DNA during oogenesis restricts the transmission of a deleterious mitochondrial variant," *Nat. Genet.*, vol. 46, no. 4, pp. 389–392, 2014, doi: 10.1038/NG.2920.

[49] C. Jakubke *et al.*, "Cristae-dependent quality control of the mitochondrial genome," *Sci. Adv.*, vol. 7, no. 36, Sep. 2021, doi: 10.1126/SCIADV.ABI8886.

[50] T. A. Kunkel and D. W. Mosbaugh, "Exonucleolytic Proofreading by a Mammalian DNA Polymerase γ," *Biochemistry*, vol. 28, no. 3, pp. 988–995, 1989, doi: 10.1021/bi00429a011.

[51] W. M. Huang and I. R. Lehman, "On the Exonuclease Activity of Phage T4 Deoxyribonucleic Acid Polymerase," *J. Biol. Chem.*, vol. 247, no. 10, pp. 3139–3146, May 1972, doi: 10.1016/S0021-9258(19)45224-1.

[52] B. Macao *et al.*, "The exonuclease activity of DNA polymerase γ is required for ligation during mitochondrial DNA replication," *Nat. Commun.*, vol. 6, Jun. 2015, doi: 10.1038/NCOMMS8303.

[53] D. A. Clayton, J. N. Doda, and E. C. Friedberg, "The absence of a pyrimidine dimer repair mechanism in mammalian mitochondria," *Proc. Natl. Acad. Sci. U. S. A.*, vol. 71, no. 7, pp. 2777–2781, 1974, doi: 10.1073/PNAS.71.7.2777.

[54] M. Alexeyev, I. Shokolenko, G. Wilson, and S. LeDoux, "The maintenance of mitochondrial DNA integrity--critical analysis and update," *Cold Spring Harb. Perspect. Biol.*, vol. 5, no. 5, 2013, doi: 10.1101/CSHPERSPECT.A012641.

[55] J. P. Van Dijken *et al.*, "An interlaboratory comparison of physiological and genetic properties of four Saccharomyces cerevisiae strains," *Enzyme Microb. Technol.*, vol. 26, no. 9–10, pp. 706–714, Jun. 2000, doi: 10.1016/S0141-0229(00)00162-9.

[56] M. S. Longtine *et al.*, "Additional Modules for Versatile and Economical PCR-based

Gene Deletion and Modification in Saccharomyces cerevisiae," □□□□□ *Yeast*, vol. 14, pp. 953–961, 1998, doi: 10.1002/(SICI)1097-0061(199807)14:10.

[57] A. P. Rosebrock, "Synchronization and Arrest of the Budding Yeast Cell Cycle Using Chemical and Genetic Methods," *Cold Spring Harb. Protoc.*, vol. 2017, no. 1, p. pdb.prot088724, Jan. 2017, doi: 10.1101/PDB.PROT088724.

[58] S. B. Haase and S. I. Reed, "Improved Flow Cytometric Analysis of the Budding Yeast Cell Cycle," *Cell Cycle*, vol. 1, no. 2, pp. 117–121, 2002, doi: 10.4161/cc.1.2.114.

[59] F. Padovani, B. Mairhörmann, P. Falter-Braun, J. Lengefeld, and K. M. Schmoller, "Segmentation, tracking and cell cycle analysis of live-cell imaging data with Cell-ACDC," *BMC Biol.*, vol. 20, no. 1, Dec. 2022, doi: 10.1186/S12915-022-01372-6.

[60] A. Chaudhry, R. Shi, and D. S. Luciani, "A pipeline for multidimensional confocal analysis of mitochondrial morphology, function, and dynamics in pancreatic β-cells," *Am. J. Physiol. - Endocrinol. Metab.*, vol. 318, no. 2, pp. E87–E101, Feb. 2020, doi: 10.1152/AJPENDO.00457.2019/ASSET/IMAGES/LARGE/ZH10022082780008.JPEG.

625 ## Main figure legends

626 **Figure 1: mtDNA damage results in mtDNA clearance**

627 **(A)** Representative images of mt-nucleoids stained with Sybr Green I (SGI). [Top] mt-
628 nucleoids in empty vector and mtDarT cells before addition of β-estradiol (0 hr). [Bottom] mt-
629 nucleoids in empty vector and mtDarT cells after addition of β-estradiol (8 hrs). Dashed lines
630 represent cell boundaries. * indicates mt-nucleoids and # indicates ρ^0 cells. **(B)** 2D density
631 correlation plots of the number of mt-nucleoids per cell against the respective cell area for
632 empty vector or mtDarT before [top] and 8 hrs post-induction [bottom]. Spearman's correlation
633 coefficient (***ρ***) is indicated in the top-left corner of each plots. Data are pooled from 3
634 independent repeats (n > 287 cells per group, per repeat). **(C)** Percentage of cells containing
635 nucleoid foci (ρ^+) in empty vector [left] or mtDarT [right] expressing cells at 0, 4 and 8 hrs
636 after induction. Data shown from 3 independent repeats (n > 207 cells per group, per repeat).
637 Mean and S.D. are shown. ns, not significant (P > 0.05) and **P ≤ 0.01 by unpaired t-test. **(D)**
638 Density distributions for the number of nucleoids per cell in empty vector [left] and mtDarT
639 [right] before (0 hr) and after (4, 8 hrs) induction. Data are pooled from 3 independent repeats
640 (n > 273 cells per group, per repeat). Scale bar, 8μm here, and in all other images. Statistical
641 tests and exact P values for all graphs are provided in Table S5.

642 **Figure 2: mtDNA loss occurs independent of cell cycle progression**

643 **(A)** Experimental setup followed for inducing mtDNA damage under cell cycle arrest using α-
644 factor in Δ*bar1* cells. Representative images of nucleoids in asynchronous and arrested cells
645 are shown. Flow cytometry profiles of cell cycle stages in asynchronous and arrested cells are
646 also provided. **(B)** Representative images of mt-nucleoid foci in G1/S arrested cells. [Top]
647 empty vector and mtDarT expressing cells at 0 hr. [Bottom] empty vector and mtDarT
648 expressing cells at 8 hrs. **(C)** Percentage of cells containing nucleoid foci (ρ^+) in empty vector
649 [left] or mtDarT [right] expressing cells at 0, 4 and 8 hrs after induction in G1/S arrest cells.
650 Data shown from 3 independent repeats (n > 61 cells per group, per repeat). Mean and S.D. are
651 shown. ns, not significant (P > 0.05), *P ≤ 0.05 by unpaired t-test. **(D)** Density distributions for
652 the number of nucleoids per cell in empty vector [left] and mtDarT [right] expressing cells
653 before (0 hr) and after (4, 8 hrs) induction in G1/S arrest cells. Data are pooled from 4
654 independent repeats (n > 50 cells per group, per repeat). Inset in mtDarT shows distribution
655 upto 50 nucleoids/cell. **(E-F)** 2D density correlation plots of the number of mt-nucleoids per
656 cell against the respective cell area for empty vector or mtDarT before [E] and 8 hrs post-

657 induction [F]. Spearman's correlation coefficient (***ρ***) is indicated in the top-left corner of each
658 plots. Data are pooled from 4 independent repeats (n > 50 cells per group, per repeat).

659 **Figure 3: mtDNA loss is dependent on the exonuclease activity of Mip1**

660 **(A)** Schematic representing the domain organization of Mip1. Residues mutated to generate
661 *mip1*$^{exo-}$ mutant are indicated. Schematic created with Biorendor.com. **(B)** Representative
662 images of mt-nucleoid foci in *mip1*$^{exo-}$ cells. [Top] empty vector and mtDarT expressing cells
663 at 0 hr. [Bottom] empty vector and mtDarT expressing cells at 8 hrs. **(C)** Percentage of *mip1*$^{exo-}$
664 cells containing nucleoid foci (ρ^+) in empty vector [left] or mtDarT [right] at 0, 4 and 8 hrs
665 after induction. Data shown from 3 independent repeats (n > 139 cells per group, per repeat).
666 Mean and S.D. are shown. ns, not significant (P > 0.05) by paired t-test. **(D)** Density
667 distributions for the number of nucleoids per cell before (0 hr) and after (4, 8 hrs) induction in
668 empty vector [left] and mtDarT [right] expressing *mip1*$^{exo-}$ cells. Data are pooled from 3
669 independent repeats (n > 88 cells per group, per repeat). **(E-F)** 2D density correlation plots of
670 the number of mt-nucleoids per cell against the respective cell area for empty vector or mtDarT
671 before [E] and 8 hrs post-induction [F] in *mip1*$^{exo-}$ cells. Spearman's correlation coefficient (***ρ***)
672 is indicated in the top-left corner of each plots. Data are pooled from 3 independent repeats (n
673 > 149 cells per group, per repeat).

674 **Figure 4: mtDNA loss is dependent on the polymerase and exonuclease domains of Mip1**

675 **(A)** Representative images of mt-nucleoid foci in *mip1*$^{exo-}$ cells expressing *mip1-CΔ669*. [Top]
676 empty vector and mtDarT expressing cells at 0 hr. [Bottom] empty vector and mtDarT
677 expressing cells at 8 hrs. **(B)** Percentage of cells containing nucleoid foci (ρ^+) in empty vector
678 [left] or mtDarT [right] at 0 and 8 hrs after induction in *mip1*$^{exo-}$ mutant expressing *mip1-*
679 *CΔ669*. Data shown from 3 independent repeats (n > 136 cells per group, per repeat). Mean
680 and S.D. are shown. Ns, not significant (P > 0.05), *P ≤ 0.05 by unpaired t-test. **(C)** Density
681 distributions for the number of nucleoids per cell in empty vector [left] or mtDarT [right] at 0
682 and 8 hrs after induction in *mip1*$^{exo-}$ mutant expressing *mip1-CΔ669* (n > 151 cells per group,
683 per repeat). **(D-F)** As (A-C) for *mip1*$^{exo-}$ cells expressing *mip1-CΔ263.*

684 **Figure 5: Rates of mtDNA loss are influenced by dNTP levels**

685 **(A)** Density distributions of the number of nucleoids per cell [left] or cell area [right] between
686 wild type and *Δsml1* cells in the absence of damage. Data shown from 3 independent repeats
687 (n > 287 cells per group, per repeat). **(B)** Percentage of cells containing nucleoid foci (ρ^+) in
688 empty vector [left] or mtDarT [right] at 0, 4 and 8 hrs after induction in *Δsml1* cells. Mean and
689 S.D. are shown. ns, not significant (P > 0.05), **P ≤ 0.01 and ***P ≤ 0.001 by unpaired t-test.
690 Data shown from 3 independent repeats (n > 203 cells per group, per repeat). **(C)** Density

691 distributions for the number of nucleoids per cell in empty vector [left] or mtDarT [right] at 0
692 and 8 hrs after induction in *Δsml1* cells. (n > 303 cells per group, per repeat).

693 ## Supplementary figure legends

694 **Figure S1: mtDNA damage results in mtDNA clearance**

695 **(A)** Experimental setup followed for inducing mtDNA damage using the mtDarT system is
696 shown [27]. Schematic created with Biorendor.com. **(B)** Representative Western blot of
697 mtDarT-3x-Flag cells before (0 hr) and after (4, 8 hrs) 100nM β-estradiol addition. Whole cell
698 lysate is probed with Coomassie as loading control (n=3 independent repeats). **(C)** Survival of
699 yeast cells with empty vector or mtDarT plasmid, grown on media with and without 50nM β-
700 estradiol. Representative image from 3 independent repeats is shown. **(D)** Representative
701 images of mt-nucleoids stained with SGI and mitochondria marked with Cox4-mCherry. **(E)**
702 SGI staining in Δ*fzo1* cells (ρ^0, mtDNA absent). **(F)** Western blot of Cox4-mCherry in empty
703 vector and mtDarT cells, before (0 hr) and after (4, 8 hrs) damage induction. Representative
704 western blot image is shown on the [left] and levels are quantified on the [right]. n=3
705 independent repeats. Mean and S.D. are shown. ns, not significant by unpaired t-test.

706 **Figure S2: mtDNA loss occurs independent of cell cycle progression**

707 **(A)** Representative images of mt-nucleoid foci in G2/M arrested empty vector and mtDarT
708 expressing cells at 0 hr [Top] and 8 hrs after induction of mtDarT [Bottom]. **(B)** Percentage of
709 cells containing nucleoid foci (ρ^+) in empty vector [left] or mtDarT [right] expressing cells at
710 0 and 8 hrs after induction in G2/M-arrested cells. Data shown from 3 independent repeats (n
711 > 133 cells per group, per repeat). Mean and S.D. are shown. Ns, not significant ($P > 0.05$),
712 ***$P \leq 0.001$ by unpaired t-test.

713 **Figure S3: mtDNA loss is dependent of the exonuclease activity of Mip1**

714 **(A)** 2D density correlation plots of the number of mt-nucleoids per cell against the respective
715 cell area for empty vector or mtDarT before [top] and 8 hrs post-induction [bottom] in Δ*nuc1*
716 cells. Spearman's correlation coefficient (***ρ***) is indicated in the top-left corner of each plots.
717 Data are pooled from 3 independent repeats (n >181 cells per group, per repeat). **(B)** Percentage
718 of Δ*nuc1* cells containing nucleoid foci (ρ^+) in empty vector [left] or mtDarT [right] at 0 and 8
719 hrs after induction. Data shown from 3 independent repeats (n > 125 cells per group, per
720 repeat). Mean and S.D. are shown. Ns, not significant ($P > 0.05$), ****$P \leq 0.0001$ by unpaired
721 t-test. **(C)** Western blot of Mip1 mNeonGreen [top] and *mip1*$^{exo-}$ mNeonGreen [bottom] before
722 (0 hr) and after (4, 8 hrs) damage induction. Representative western blot image is shown on the
723 [left] and levels are quantified on the [right].N=3 independent repeats. Mean and S.D. are
724 shown. Ns, not significant $P > 0.05$, *$P \leq 0.05$ by unpaired t-test.

725 **Figure S4: mtDNA loss is dependent on the polymerase and exonuclease domains of Mip1**
726 **(A)** Western blot of Mip1-mNeonGreen, Mip1-CΔ263-mNeonGreen and Mip1-CΔ669-
727 mNeonGreen. Representative image is shown from one of the 3 independent repeats. **(B)** [Left]
728 Localization of Mip1-CΔ263-mNeonGreen (i) or Mip1-CΔ669-mNeonGreen (ii) and mt-
729 nucleoids stained with DAPI in *mip1*$^{exo-}$ cells. [Right] Line profiles of Mip1-CΔ263-
730 mNeonGreen (i) or Mip1-CΔ669-mNeonGreen (ii) and mt-nucleoids stained with DAPI in
731 *mip1*$^{exo-}$ cells. Line profile for a representative across an ROI is shown (yellow line in merged
732 panel).
733 **Figure S5: Rates of mtDNA loss are influenced by dNTP levels (A)** Western blot of Mip1-
734 mNeonGreen Δ*sml1* cells before (0 hr) and after (4, 8 hrs) damage induction. Representative
735 Western blot image is shown on the [left] and levels are quantified on the [right]. n=3
736 independent repeats. Mean and S.D. are shown. n.s., not significant $P > 0.05$ by unpaired t-test.
737 **(B)** Serial dilution growth assay to measure growth of *Δsml1* cells in comparison to a wild type
738 control. Representative image from 3 independent repeats is shown. **(C)** Percentage of cells
739 containing nucleoid foci (ρ^+) in empty vector [left] or mtDarT [right] at 0, 4 and 8 hrs after
740 induction in Δ*sml1 mip1*$^{exo-}$ background. Data shown from 3 independent repeats ($n > 139$ cells
741 per group, per repeat). Mean and S.D. are shown. Ns, not significant ($P > 0.05$) by unpaired t-
742 test. **(D)** Density distributions for the number of nucleoids per cell in empty vector [left] or
743 mtDarT [right] at 0, 4 and 8 hrs after induction in *Δsml1 mip1*$^{exo-}$ cells. ($n > 179$ cells per group,
744 per repeat).
745

Figure 1

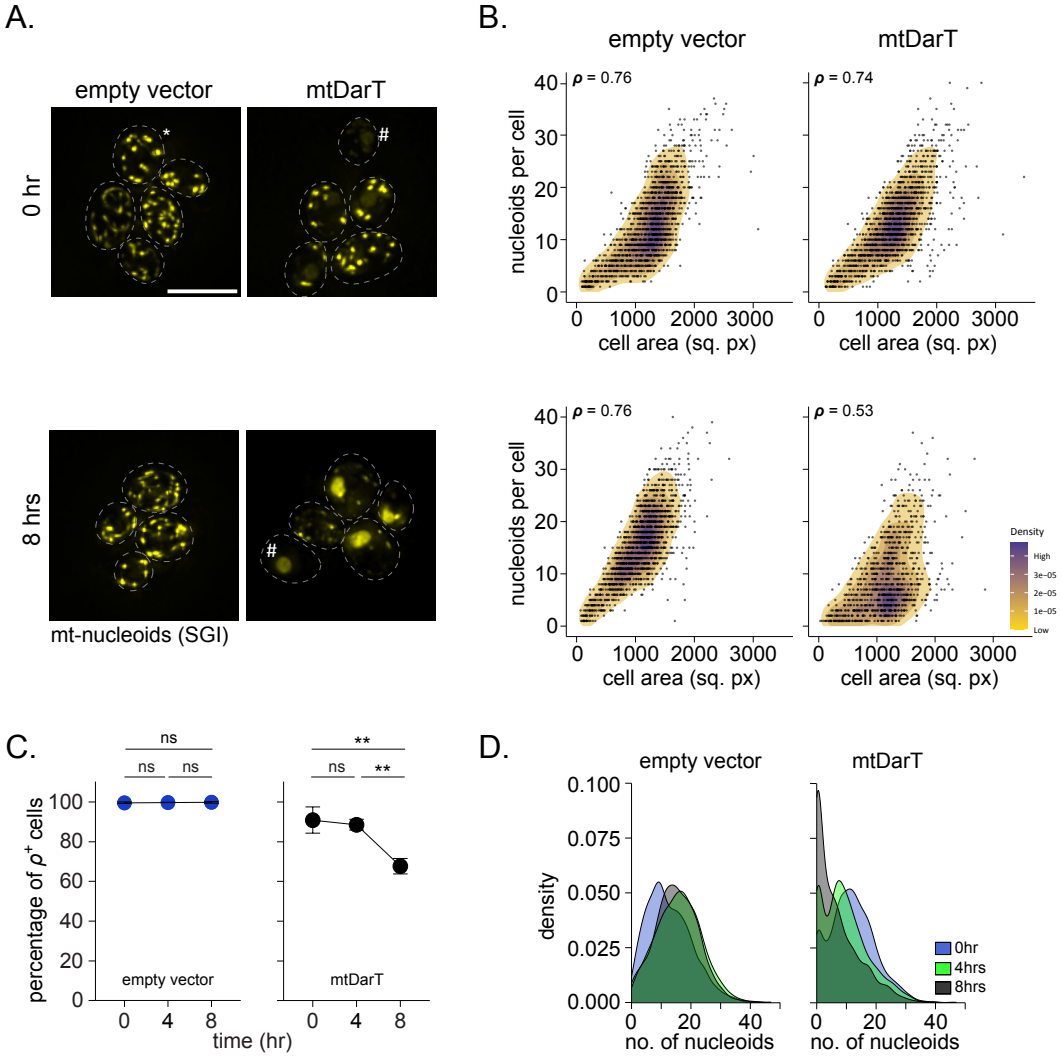
A.
empty vector
mtDarT
0 hr
8 hrs
mt-nucleoids (SGI)
B.
empty vector
mtDarT
ρ = 0.76
ρ = 0.74
ρ = 0.76
ρ = 0.53
nucleoids per cell
cell area (sq. px)
Density
High
Low
C.
ns
ns
ns
**
ns
**
percentage of ρ+ cells
empty vector
mtDarT
time (hr)
D.
empty vector
mtDarT
density
no. of nucleoids
0hr
4hrs
8hrs

Figure 2

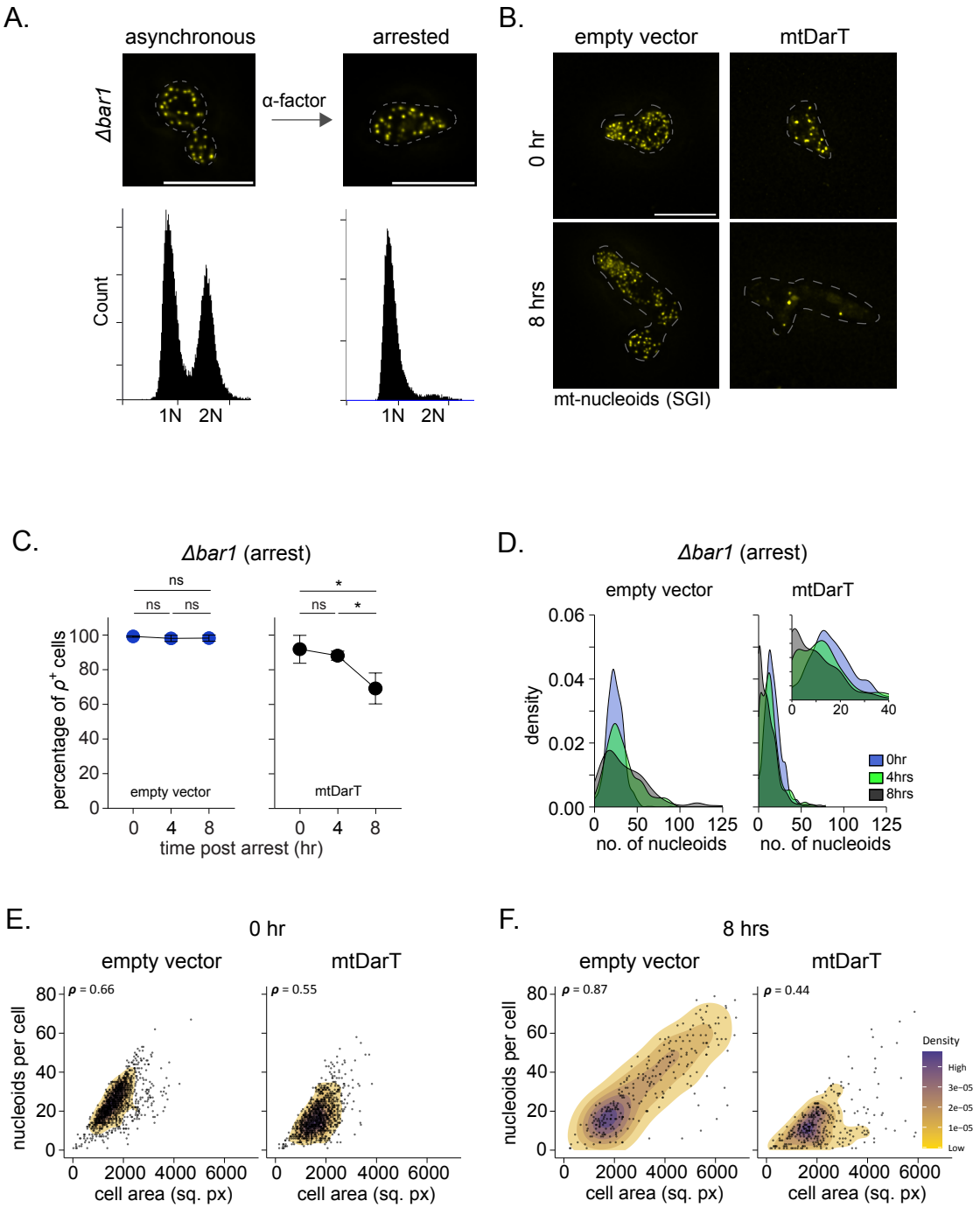
A.
asynchronous
arrested
Δbar1
α-factor
Count
1N 2N
1N 2N
B.
empty vector
mtDarT
0 hr
8 hrs
mt-nucleoids (SGI)
C.
Δbar1 (arrest)
ns
ns ns
*
ns *
percentage of ρ+ cells
100
80
60
40
20
0
empty vector
mtDarT
0 4 8
0 4 8
time post arrest (hr)
D.
Δbar1 (arrest)
empty vector
mtDarT
density
0.06
0.04
0.02
0.00
0 20 40
0hr
4hrs
8hrs
0 50 100 125
0 50 100 125
no. of nucleoids
no. of nucleoids
E.
0 hr
empty vector
mtDarT
ρ = 0.66
ρ = 0.55
nucleoids per cell
80
60
40
20
0
0 2000 4000 6000
0 2000 4000 6000
cell area (sq. px)
cell area (sq. px)
F.
8 hrs
empty vector
mtDarT
ρ = 0.87
ρ = 0.44
nucleoids per cell
Density
High
3e−05
2e−05
1e−05
Low
0 2000 4000 6000
0 2000 4000 6000
cell area (sq. px)
cell area (sq. px)

Figure 3

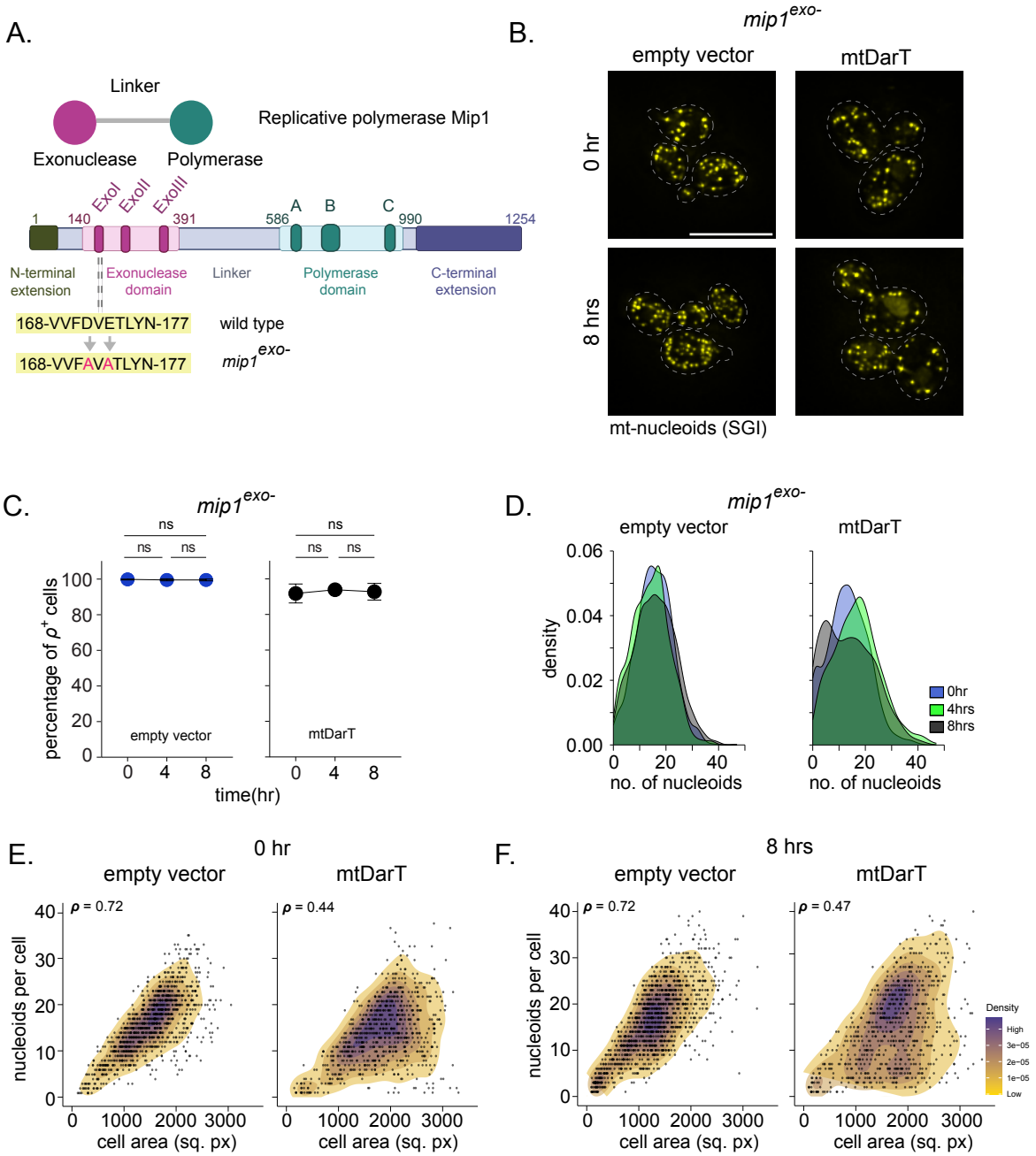
A.
Linker
Replicative polymerase Mip1
Exonuclease
Polymerase
ExoI
ExoII
ExoIII
1
140
391
586
990
1254
A
B
C
N-terminal extension
Exonuclease domain
Linker
Polymerase domain
C-terminal extension
168-VVFDVETLYN-177
wild type
168-VVFAVATLYN-177
mip1exo-
B.
mip1exo-
empty vector
mtDarT
0 hr
8 hrs
mt-nucleoids (SGI)
C.
mip1exo-
ns
percentage of ρ+ cells
empty vector
mtDarT
time(hr)
D.
mip1exo-
empty vector
mtDarT
density
0hr
4hrs
8hrs
no. of nucleoids
E.
0 hr
empty vector
mtDarT
ρ = 0.72
ρ = 0.44
nucleoids per cell
cell area (sq. px)
F.
8 hrs
empty vector
mtDarT
ρ = 0.72
ρ = 0.47
Density
High
Low

Figure 4

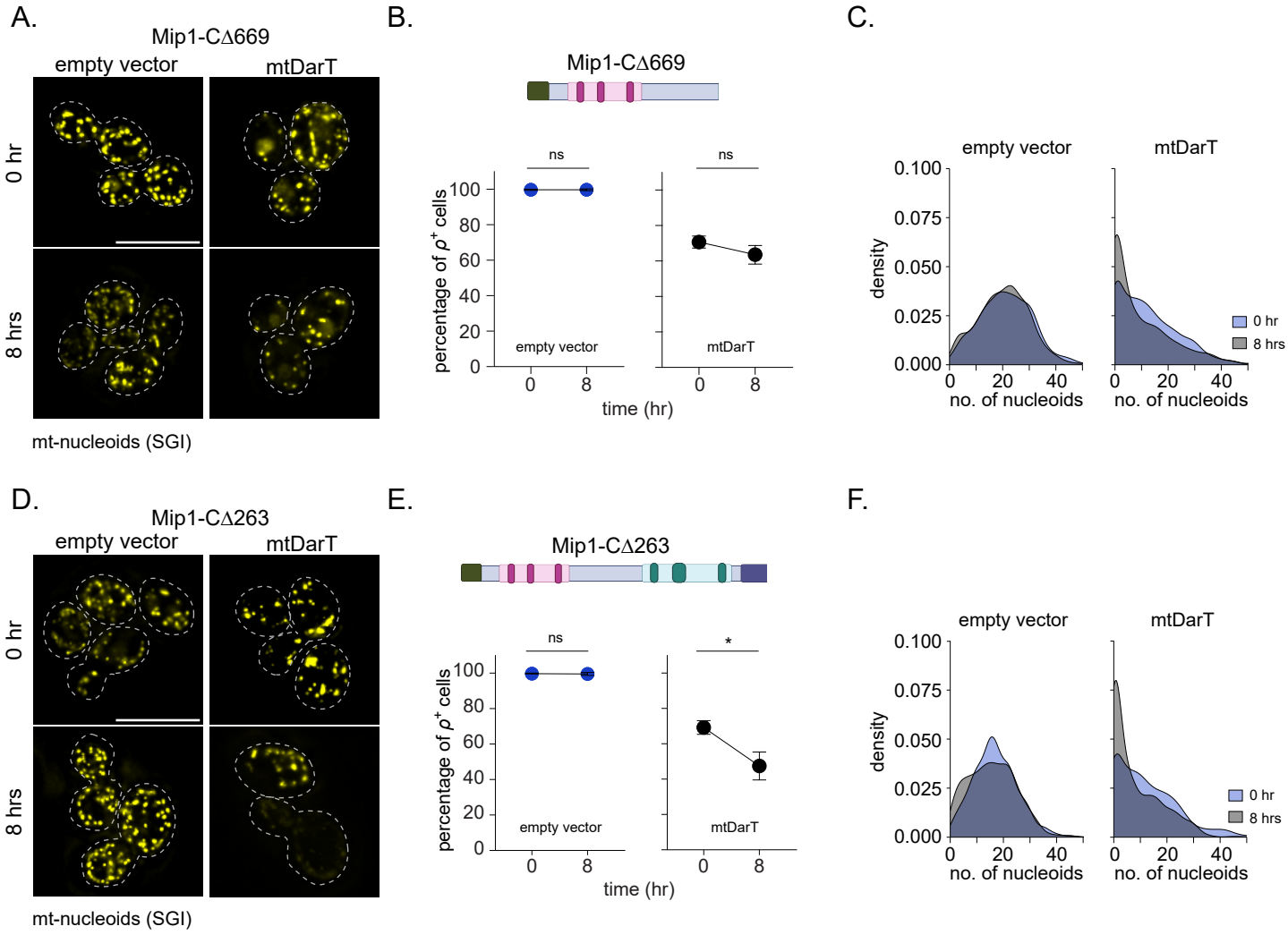
A.
Mip1-CΔ669
empty vector
mtDarT
0 hr
8 hrs
mt-nucleoids (SGI)
B.
Mip1-CΔ669
ns
ns
percentage of ρ+ cells
100
80
60
40
20
0
empty vector
mtDarT
0
8
0
8
time (hr)
C.
empty vector
mtDarT
density
0.100
0.075
0.050
0.025
0.000
0
20
40
no. of nucleoids
0 hr
8 hrs
D.
Mip1-CΔ263
empty vector
mtDarT
0 hr
8 hrs
mt-nucleoids (SGI)
E.
Mip1-CΔ263
ns
*
percentage of ρ+ cells
empty vector
mtDarT
time (hr)
F.
empty vector
mtDarT
density
no. of nucleoids
0 hr
8 hrs

Figure 5

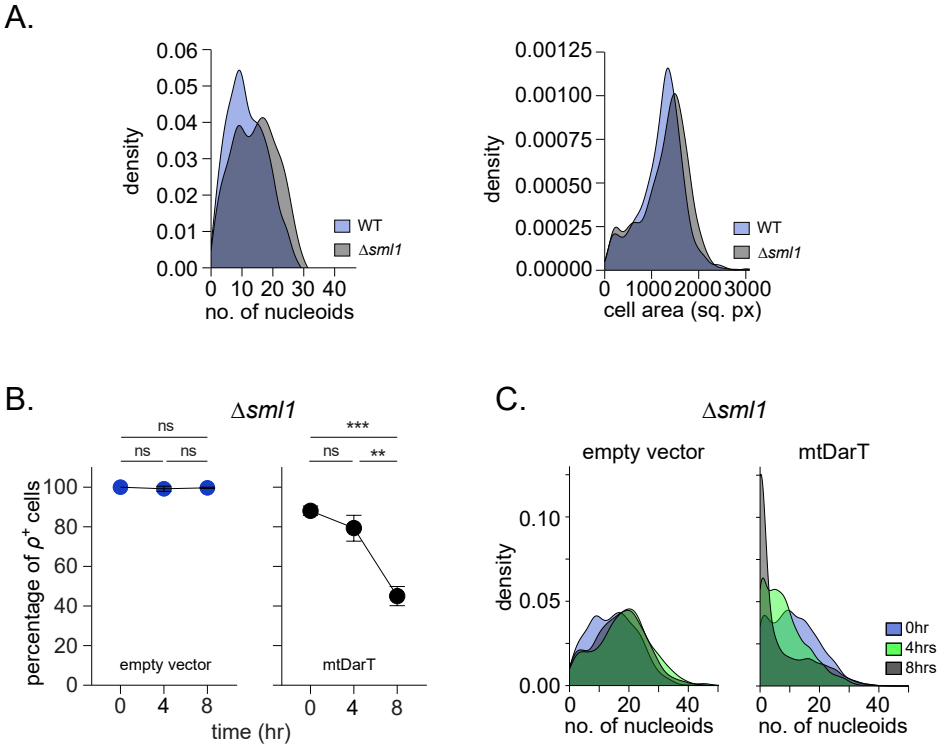
A.
density
no. of nucleoids
WT
Δsml1
cell area (sq. px)
B.
Δsml1
ns
***
**
percentage of ρ+ cells
empty vector
mtDarT
time (hr)
C.
Δsml1
empty vector
mtDarT
0hr
4hrs
8hrs

Figure S1

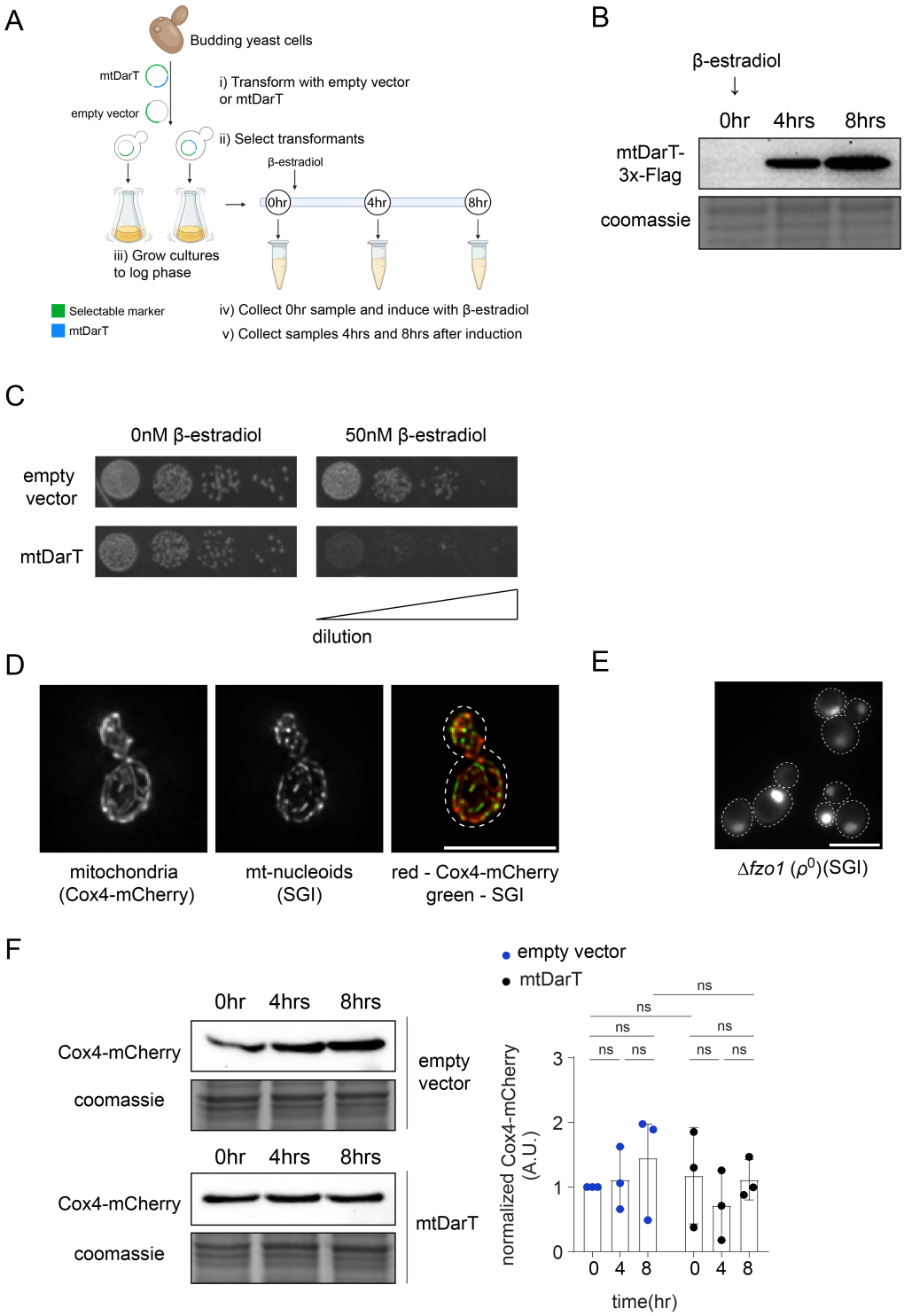
A
Budding yeast cells
mtDarT
empty vector
i) Transform with empty vector or mtDarT
ii) Select transformants
β-estradiol
0hr
4hr
8hr
iii) Grow cultures to log phase
Selectable marker
mtDarT
iv) Collect 0hr sample and induce with β-estradiol
v) Collect samples 4hrs and 8hrs after induction
B
β-estradiol
0hr 4hrs 8hrs
mtDarT-3x-Flag
coomassie
C
0nM β-estradiol
50nM β-estradiol
empty vector
mtDarT
dilution
D
mitochondria (Cox4-mCherry)
mt-nucleoids (SGI)
red - Cox4-mCherry
green - SGI
E
Δfzo1 (ρ0)(SGI)
F
0hr 4hrs 8hrs
Cox4-mCherry
coomassie
empty vector
mtDarT
empty vector
mtDarT
ns
normalized Cox4-mCherry (A.U.)
time(hr)

Figure S2

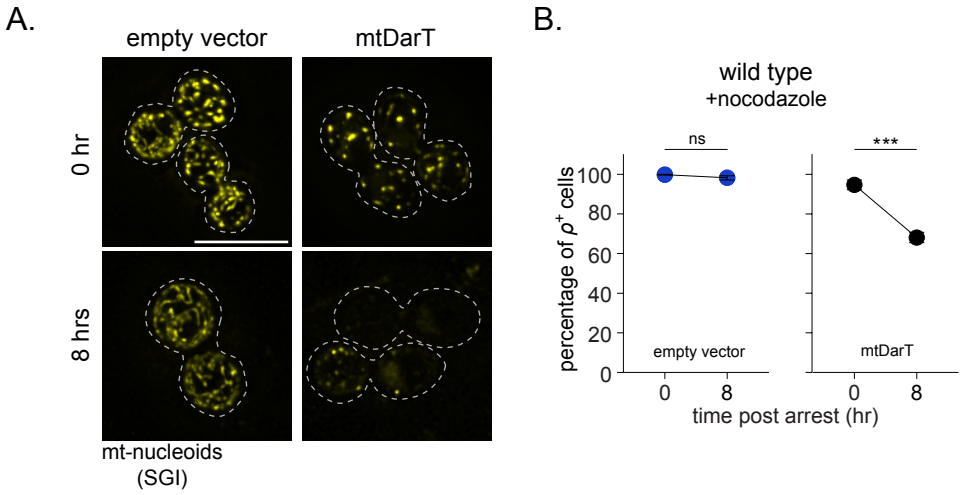
A.
empty vector
mtDarT
0 hr
8 hrs
mt-nucleoids
(SGI)
B.
wild type
+nocodazole
ns
***
percentage of ρ+ cells
100
80
60
40
20
0
empty vector
mtDarT
0
8
0
8
time post arrest (hr)

Figure S3

A.

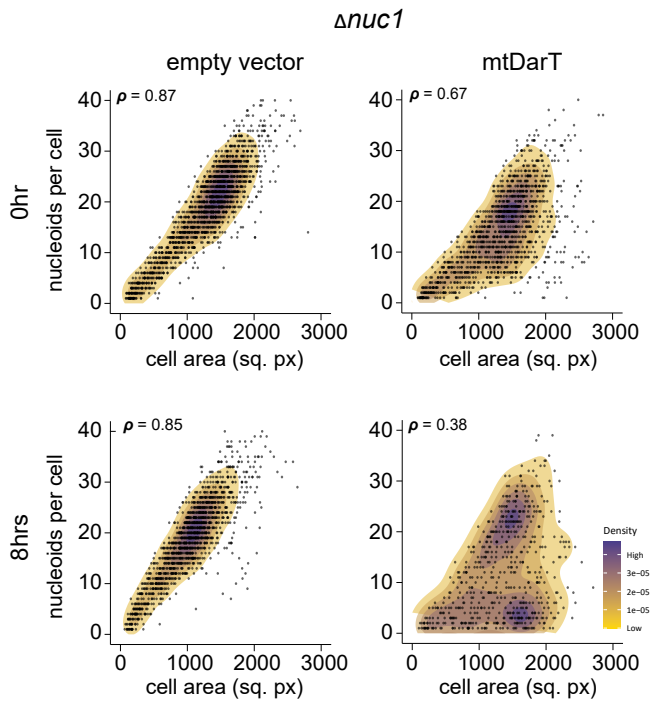

B.

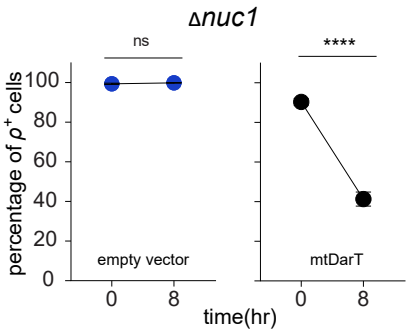

C.

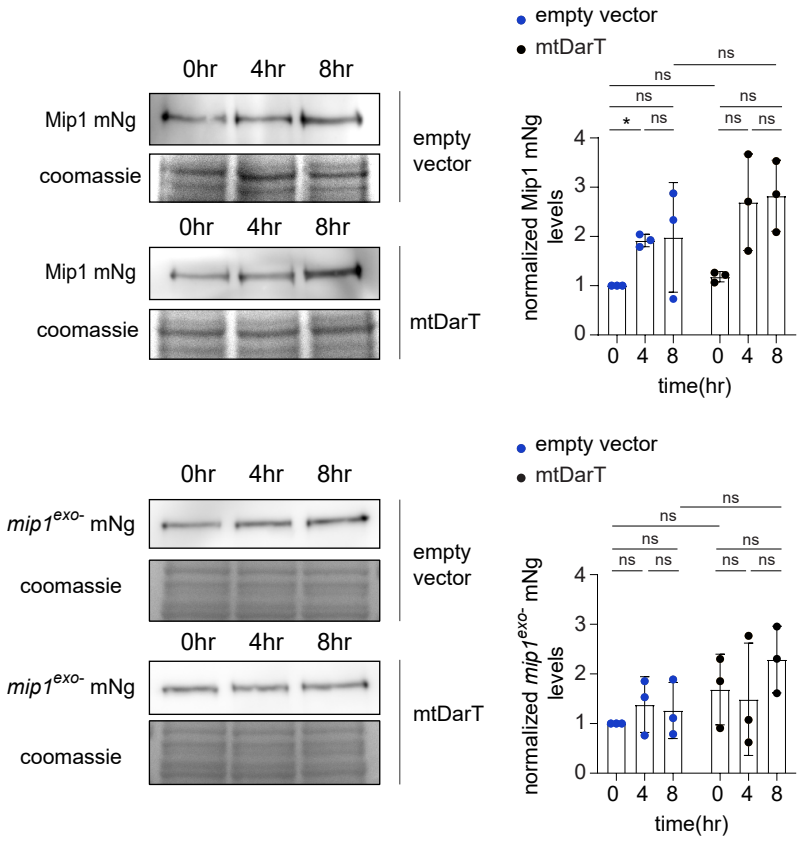

Figure S4

A.

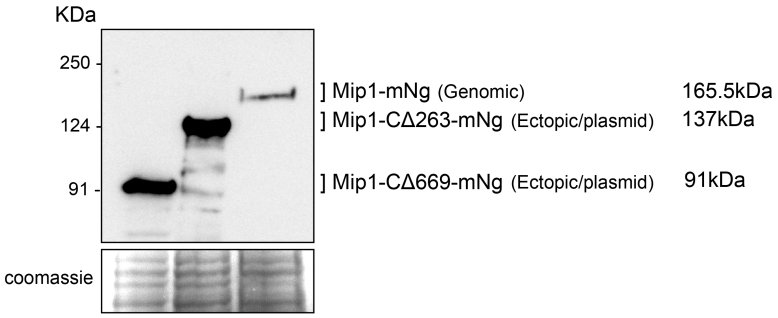
KDa
250
124
91
coomassie
] Mip1-mNg (Genomic)
] Mip1-CΔ263-mNg (Ectopic/plasmid)
] Mip1-CΔ669-mNg (Ectopic/plasmid)
165.5kDa
137kDa
91kDa

B.

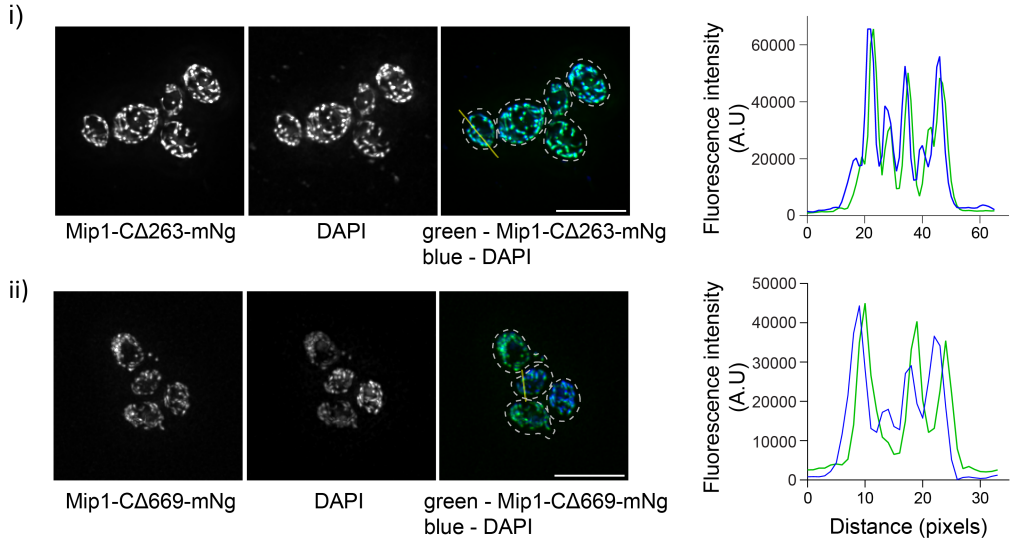
i)
Mip1-CΔ263-mNg
DAPI
green - Mip1-CΔ263-mNg
blue - DAPI
Fluorescence intensity (A.U)
60000
40000
20000
0
0
20
40
60
ii)
Mip1-CΔ669-mNg
DAPI
green - Mip1-CΔ669-mNg
blue - DAPI
Fluorescence intensity (A.U)
50000
40000
30000
20000
10000
0
0
10
20
30
Distance (pixels)

Figure S5

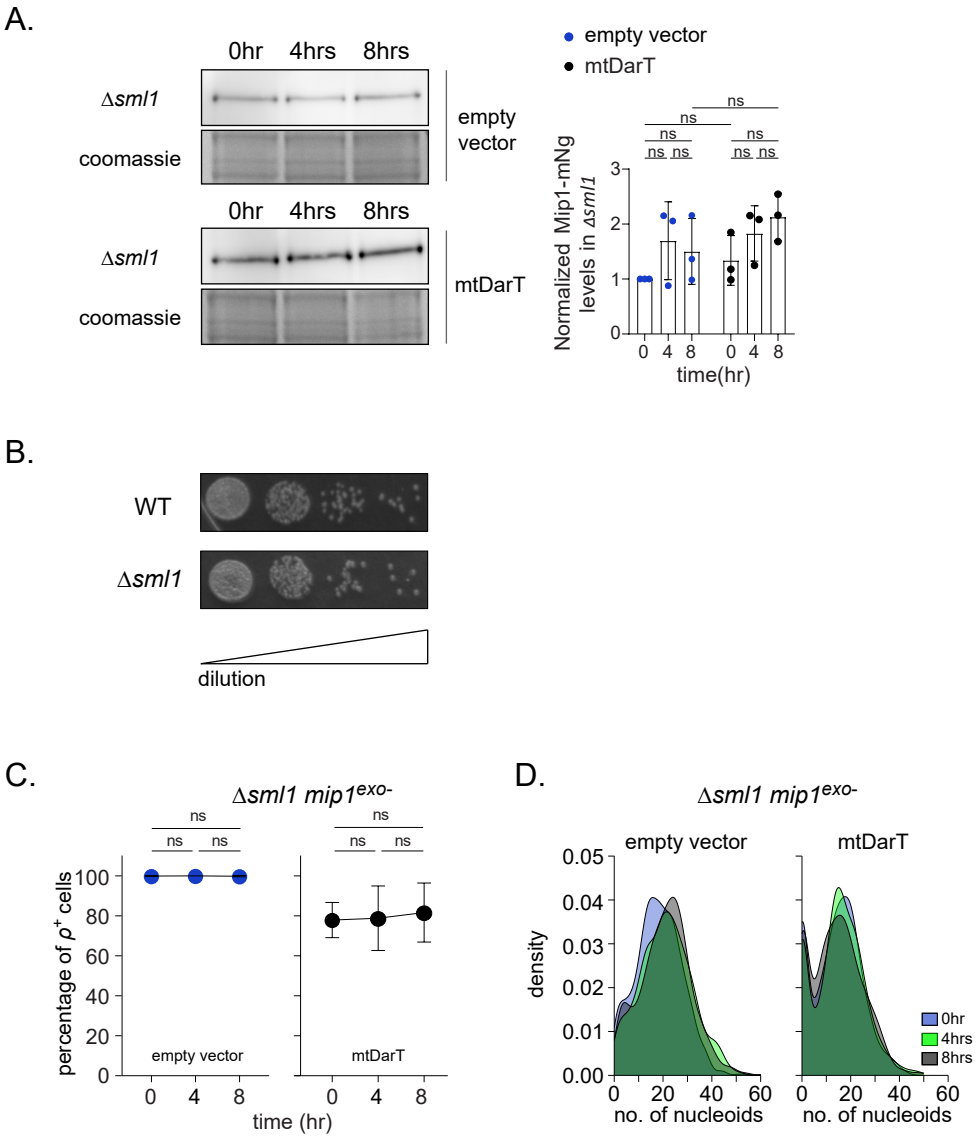
A.
0hr 4hrs 8hrs
Δsml1
coomassie
empty vector
0hr 4hrs 8hrs
Δsml1
coomassie
mtDarT
empty vector
mtDarT
ns
Normalized Mip1-mNg levels in Δsml1
time(hr)
B.
WT
Δsml1
dilution
C.
Δsml1 mip1exo-
ns
percentage of p+ cells
empty vector
mtDarT
time (hr)
D.
Δsml1 mip1exo-
empty vector
mtDarT
density
0hr
4hrs
8hrs
no. of nucleoids

Table S1. Strains used in this study

Strain	Stain ID	Genotype	Description	Source
CEN.PK	NABC567	*MAT***a**	Prototrophic yeast strain	[1]
CEN.PK	NABC568	*MAT*α	Prototrophic yeast strain	[1]
Δ*bar1*	NABC595	*MAT***a** Δ*bar1*::*Hyg*		Dr. Sunil Laxman Lab
Δ*sml1*	NABC639	*MAT*α *Δsml1::Hyg*	pNABC552 was used to amplify the HygR cassette together with overhangs for Sml1, ND_489 and ND_490. Transformants were screened and confirmed for *Δsml1* using ND_488 and AS_81.	This study
Δ*nuc1*	NABC641	*MAT***a** *Δnuc1::KanMX6*	pNABC551 was used to amplify the KanR cassette together with overhangs for Nuc1, AS_92 and AS_93. Transformants were screened and confirmed for *Δnuc1* using AS_91 and AS_81.	This study
Mip1-mCherry	NABC772	*MAT***a** *Mip1-mCherry-Hyg*	pNABC549 was used to amplify the mCherry-HygR cassette together with overhangs for Mip1, AS_79 and AS_80. Transformants were screened and confirmed for Mip1 C-ter tagging using AS_78 and AS_81.	This study
Mip1 mNeongreen	NABC773	*MAT***a** *Mip1-mNeongreen-KanMX6*	pNABC553 was used to amplify the mNeonGreen-KanR cassette together with overhangs for Mip1, AS_79 and AS_80. Transformants were screened and confirmed for Mip1 C-ter tagging using AS_78 and AS_81.	This study
Mip1^{exo-}	NABC573	*MAT***a** *mip1Δ::mip1^{D171A,E173A}-Hyg*	Exonuclease-deficient Mip1 mutant (Mip1^{exo-}) was constructed as previously described [2], [3]. The mutant harbors two tandem mutations, D171A and E173A, in the ExoI motif of the exonuclease domain. The mutations were introduced by site-directed mutagenesis where the endogenous copy of Mip1 was deleted and subsequently transformed with a gene fragment containing Mip1 D171A, E173A double-mutation. Insertion of the mutant fragment was confirmed by sequencing. Deletion of Mip1 renders a cell ρ^0. Therefore, mtDNA was reintroduced into Mip1^{exo-} mutants by crossing with wild type cells of opposite mating-type. Haploid spores were dissected to obtain Mip1^{exo-}mutants with mtDNA**.**	This study
Mip1^{exo-} mNeongreen	NABC680	*MAT***a** *mip1Δ::mip1^{D171A,E173A}-mNeongreen-KanMX6*	Same as NABC773, but in Mip1^{exo}- cells.	This study
Δ*sml1* Mip1-mNeongreen	NABC766	*MAT***a** *sml1Δ::Hyg Mip1-mNeongreen::KanMX6*	Same as NABC773, but in NABC639 cells.	This study
Cox4-mCherry	NABC569	*MAT***a** *Cox4-mCherry-Hyg*	pNABC549 was used to amplify the mCherry-HygR cassette together with overhangs for Cox4, ND_328 and ND_329. Transformants were screened and confirmed for Cox4 C-ter tagging using ND_327 and AS_81.	This study

References:

[1] J. P. Van Dijken *et al.*, “An interlaboratory comparison of physiological and genetic properties of four Saccharomyces cerevisiae strains,” *Enzyme Microb. Technol.*, vol. 26, no. 9–10, pp. 706–714, Jun. 2000, doi: 10.1016/S0141-0229(00)00162-9.

[2] M. K. Strand, G. R. Stuart, M. J. Longley, M. A. Graziewicz, O. C. Dominick, and W. C. Copeland, “POS5 gene of Saccharomyces cerevisiae encodes a mitochondrial NADH kinase required for stability of mitochondrial DNA,” *Eukaryot. Cell*, vol. 2, no. 4, pp. 809–820, Aug. 2003, doi: 10.1128/EC.2.4.809-820.2003/ASSET/B99DBC2E-8E6C-493C-A757-392BBCBDDE25/ASSETS/GRAPHIC/EK0430086007.JPEG.

[3] T. C. Medeiros and M. Graef, “Autophagy determines mtDNA copy number dynamics during starvation,” *Autophagy*, vol. 15, no. 1. Taylor and Francis Inc., pp. 178–179, Jan. 02, 2019. doi: 10.1080/15548627.2018.1532263.

Table S2. Plasmids used in this study

Plasmid	Description	Construct details	Source
pNABC552	DH5α pFA6a-KO-Hyg	Plasmid for gene deletion in S. cerevisiae (hyg^R).	Dr. Sunil Laxman Lab
pNABC551	DH5α pFA6a-KO-KanMX6	Plasmid for gene deletion in S. cerevisiae (kan^R).	Dr. Sunil Laxman Lab
pNABC549	DH5α pFA6a-mCherry-Hyg	Plasmid for C-ter tagging of genes with mCherry in S. cerevisiae (hyg^R).	Dr. Sunil Laxman Lab
pNABC553	DH5α pFA6a-mNeongreen-Kan	Plasmid for C-ter tagging of genes with mNeongreen in S. cerevisiae (kan^R).	This study
NABC557	DH5α pGEV-3XFlag-NAT	Plasmid for inducible overexpression of a gene of interest with C-ter Flag tagging in S. cerevisiae (ntc^R).	AB Lab, Dua et al, 2022
pNABC561	DH5α pGEV-Su9-DarT-3XFlag-NAT	Plasmid containing Su9-DarT cloned at the PacI site downstream of pGAL1 and in frame with the linker-3XFlag sequence in NABC557 background.	AB Lab, Dua et al, 2022
pNABC555	DH5α p417-cyc1-Kan	CEN/ARS plasmid, with cyc1 promoter for low expression of protein in S. cerevisiae (kan^R).	Dr. Sunil Laxman Lab
pNABC775	DH5α pMip1-Mip1-CΔ263 in NABC555 background	Plasmid containing Mip1-CΔ263 sequence expressed under pMip1 was generated through PCR amplification of the pMip1-Mip1-CΔ263 fragment (ending at Ser991 in Mip1) from yeast genomic DNA using primers AS188 and AS202. A stop codon was introduced at the end of the truncation after residue no 991. This fragment was gibson cloned into pNABC555 in between SacI and BamHI sites (removing cyc1 promoter).	This study
pNABC777	DH5α pCYC1-Mip1-CΔ263-mNeongreen in NABC555 background	A mNeongreen tagged variant of Mip1-CΔ263 was generated by combining (Gibson cloning) the Mip1-CΔ263 fragment (amplified using AS182 and AS163 from the genomic DNA), with a fragment containing 10 aminoacid linker followed by mNeongreen sequence (amplified using AS184 and AS185). The above fragment was Gibson cloned into pNABC555 at the XbaI site.	This study
pNABC776	DH5α pMip1-Mip1-CΔ669 with stop codon in NABC555 background	Plasmid containing Mip1-CΔ669 sequence expressed under pMip1 was generated by PCR amplifying pMip1-Mip1-CΔ669 fragment (ending at Ser585 in Mip1) from yeast genomic DNA using AS188 and AS213. A stop codon was introduced at the end of the truncation after residue no 585. This fragment was Gibson cloned into pNABC555 in between SacI and BamHI sites (removing CYC1 promoter).	This study
pNABC778	DH5α pMip1-Mip1-ΔC669-mNeongreen in NABC555 background	A mNeongreen tagged variant of Mip1-CΔ669 was generated by combining Mip1-CΔ669 fragment (amplified using AS188 and AS190) with mNeongreen (amplified using AS191, AS 192). The above fragment was Gibson cloned into pNABC555 at the XbaI site.	This study

Table S3. Oligos used in this study

Primer name	Sequence
AS_188	CCCTCACTAAAGGGAACAAAAGCTGGAGCTCGCAGAAAGAACCTTCAACCTCATTTTGTT
AS_202	GATATCGAATTCCTGCAGCCCGGGGGATCCCTAGCTGTCGATATCGAGATTTGGTT
AS_184	GGCAGCGGCAGCAGCGCGAGCGGCGGCAGCATGGCTTCTTTGCCAGCTACTC
AS_183	GCTGCCGCCGCTCGCGCTGCTGCCGCTGCCGCTGTCGATATCGAGATTTGGTTTACC
AS_182	CGCAAACACAAATACACACACTAATCTAGAATGACGAAATTGATGGTTAGATCTGA
AS_185	CTGCAGCCCGGGGGATCCACTAGTTCTAGATCAAGAATTAGAAGAAGCAGAACCT
AS_213	GATATCGAATTCCTGCAGCCCGGGGGATCCTCATGACTCAGATTTTAGTACGCCCTTTTCAAA
AS_191	TTTGAAAAGGGCGTACTAAAATCTGAGTCAATGGCTTCTTTGCCAGCTACTCATGAATTG
AS_192	GATATCGAATTCCTGCAGCCCGGGGGATCCTCAAGAATTAGAAGAAGCAGAACCTGAACC
AS_190	CAATTCATGAGTAGCTGGCAAAGAAGCCATTGACTCAGATTTTAGTACGCCCTTTTCAAA
ND_334	GGGATTATATGTAGTTGTTGAGCAACGAGGGACAAGTATGCGGATCCCCGGGTTAATTAA
ND_335	ATATAAATACAAATGCGAAAGCTAATGCAGATTTTGCCTAGAATTCGAGCTCGTTTAAAC
AS_112	ATGACGAAATTGATGGTTAGATCTGAATGCATG
AS_113	CTAGTACTCTCTAGAAATAGTAATGTCCCTTTC
ND_339	TATGTAGTTGTTGAGCAACGAGGGACAAGTATGACGAAATTGATGGTTAGATCTGAATGCATGCTG
ND_340	CTGGTGGTGTTTGCTGTAGCAACACTCTATAAC
ND_341	CGTTATAGAGTGTTGCTACAGCAAACACCACCAG
ND_342	CTAGTACTCTCTAGAAATAGTAATGTCCCTTTCCAG
ND_343	AGGGACATTACTATTTCTAGAGAGTACTAGGACATGGAGGCCCAGAATACCCTCCTT
ND_344	TACAAATGCGAAAGCTAATGCAGATTTTGCCTTCGAGCGTCCCAAAACCTTCTCAAGC
ND_327	GAAAACTGCCCAAAACTTAG
ND_328	ACTAAACCCTGTTGGTGTTCCAAATGATGACCACCATCACCGGATCCCCGGGTTAATTAA
ND_329	GTAAAAGAGAAACAGAAGGGCAACTTGAATGATAAGATTAGAATTCGAGCTCGTTTAAAC
AS_78	GGAGAACAGGAGAAAGAAGG
AS_79	GGTTGAGCTGGAAAGGGACATTACTATTTCTAGAGAGTACCGGATCCCCGGGTTAATTAA
AS_80	ATATAAATACAAATGCGAAAGCTAATGCAGATTTTGCCTAGAATTCGAGCTCGTTTAAAC
ND_307	GGCATTAAATTATCGTCGTG
ND_308	TCAAAAATTGATGGTGGAAGAAATAAATTTAGACATCGATCGGATCCCCGGGTTAATTAA
ND_309	ATTGATTTGAAAAGACCTCATATATTTACAAGAATATCTAGAATTCGAGCTCGTTTAAAC
ND_488	GGCCAATGATAGGAAAGAAC
ND_489	CACTAACCTCTCTTCAACTGCTCAATAATTTCCCGCTATGCGGATCCCCGGGTTAATTAA
ND_490	AAATGGAAAGAGAAAAGAAAAGAGTATGAAAGGAACTTTAGAATTCGAGCTCGTTTAAAC
AS_91	CAAACAAGATCACCAAAAGG
AS_92	AGTTCCCCACTTATTAGATCCCAAAGTTAAAGTTATCATGCGGATCCCCGGGTTAATTAA
AS_93	TTATGAATTAATTTATATTTACAGTTTTTCAGTACATTCAGAATTCGAGCTCGTTTAAAC
AS_81	TTAATTAACCCGGGGATCCG

Table S4: Resource table

Reagent type (species) or resource	Designation	Source or reference	Catalogue number
Antibody	Rabbit Anti-Flag	Cell signalling	14793S
Antibody	Mouse Anti-mCherry	Sigma	SAB2702291
Antibody	Rabbit Anti-mNeongreen	Agrisera	AS21 4525
Antibody	Anti-rabbit IgG, HRP-linked Antibody	Cell Signaling Technology	7074S
Antibody	Anti-mouse IgG, HRP-linked Antibody	Cell Signaling Technology	7076S
Chemical/Reagent	SYBR™ Green I Nucleic Acid Gel Stain	Invitrogen	S7563
Chemical/Reagent	Molecular Probes SYTOX Green Nucleic Acid Stain	Thermo Fisher Scientific	S7020
Commercial kit	femtoLUCENT™ PLUS-HRP Chemiluminescent reagents only, 200ml	G-Biosciences	786-056
Chemical/Reagent	β-estradiol	Sigma-Aldrich	E2758
Chemical/Reagent	Ultrapure agarose	Invitrogen	16500500
Chemical/Reagent	α1-Mating Factor acetate salt	Sigma-Aldrich	T6901
Chemical/Reagent	Nocodazole	Sigma-Aldrich	487928
Chemical/Reagent	Hygromycin B	Thermo Fisher Scientific	10687010
Chemical/Reagent	Nourseothricin	Jena Bioscience	AB-102XL
Chemical/Reagent	DAPI (4',6-Diamidino-2-Phenylindole, Dihydrochloride)	Invitrogen	D1306
Chemical/Reagent	Geneticin™ Selective Antibiotic (G418 Sulfate), Powder	Thermo Fisher Scientific	11811031
Chemical/Reagent	RNAse A	Genetix	EN0531
Chemical/Reagent	Proteinase K	Invitrogen	AM2548

Table S5: Statistical tests

MAIN FIGURES								
Figure	**Panel**	**Biological replicates**	**Normality (Shapiro-Wilk Test)**	**Statistical Test**	**Spearman's correlation coefficient values(*ρ*)**	**Significance**	**Confidence interval values (CI) at 95%**	**P-value**
1	B	3	empty vector 0hr =No	Spearman's correlation coefficient (*ρ*)	0.7562311	****	12.4350313.18894	< 2.22e-16
	B	3	empty vector 8hr=No	Spearman's correlation coefficient (*ρ*)	0.7588237	****	15.0866915.80719	< 2.22e-16
	B	3	mtDarT 0hr=No	Spearman's correlation coefficient (*ρ*)	0.7391136	****	12.6674513.38938	< 2.22e-16
	B	3	mtDarT 8hr =No	Spearman's correlation coefficient (*ρ*)	0.5349318	****	8.8513889.779604	< 2.22e-16
1	C	3	empty vector 0hr=Yes, empty vector 8hr=No	Unpaired t test (Two-tailed)	NA	ns	NA	0.5169
	C	3	empty vector 0hr=Yes,empty vector 4hr=Yes	Unpaired t test (Two-tailed)	NA	ns	NA	0.6337
	C	3	empty vector 4hr=Yes, empty vector 8hr=Yes	Unpaired t test (Two-tailed)	NA	ns	NA	0.6661

	C	3	mtDarT 0hr=Yes, mtDarT 8hr=Yes	Unpaired t test (Two-tailed)	NA	**	NA	0.0061
	C	3	mtDarT 0hr=Yes, mtDarT 4hr=Yes	Unpaired t test (Two-tailed)	NA	ns	NA	0.5958
	C	3	mtDarT 4hr=Yes, mtDarT 8hr=Yes	Unpaired t test (Two-tailed)	NA	**	NA	0.0016
2	C	3	empty vector 0hr=Yes, empty vector 8hr=Yes	Unpaired t test (Two-tailed)	NA	ns	NA	0.4395
	C	3	empty vector 0hr=Yes,empty vector 4hr=Yes	Unpaired t test (Two-tailed)	NA	ns	NA	0.3957
	C	3	empty vector 4hr=Yes, empty vector 8hr=Yes	Unpaired t test (Two-tailed)	NA	ns	NA	0.9394
	C	3	mtDarT 0hr=Yes, mtDarT 8hr=Yes	Unpaired t test (Two-tailed)	NA	*	NA	0.0308
	C	3	mtDarT 0hr=Yes, mtDarT 4hr=Yes	Unpaired t test (Two-tailed)	NA	ns	NA	0.482
	C	3	mtDarT 4hr=Yes, mtDarT 8hr=Yes	Unpaired t test (Two-tailed)	NA	*	NA	0.0244
2	E	4	empty vector 0hr =No	Spearman's correlation coefficient (ρ)	0.6641275	****	23.78065 24.92036	< 2.22e-16
	E	4	mtDarT 0hr=No	Spearman's correlation	0.5548155	****	16.80136 17.97200	< 2.22e-16

				coefficient (ρ)				
2	F	4	empty vector 8hr=No	Spearman's correlation coefficient (ρ)	0.8707271	****	33.8138140.35107	< 2.22e-16
	F	4	mtDarT 8hr=No	Spearman's correlation coefficient (ρ)	0.4384645	****	12.6527215.20398	< 2.22e-16
3	C	3	empty vector 0hr=No, empty vector 8hr=Yes	Unpaired t test (Two-tailed)	NA	ns	NA	0.4182
	C	3	empty vector 0hr=Yes, empty vector 4hr=Yes	Unpaired t test (Two-tailed)	NA	ns	NA	0.5851
	C	3	empty vector 4hr=Yes, empty vector 8hr=Yes	Unpaired t test (Two-tailed)	NA	ns	NA	0.8852
	C	3	mtDarT 0hr=Yes, mtDarT 8hr=Yes	Unpaired t test (Two-tailed)	NA	ns	NA	0.8202
	C	3	mtDarT 0hr=Yes, mtDarT 4hr=Yes	Unpaired t test (Two-tailed)	NA	ns	NA	0.5584
	C	3	mtDarT 4hr=Yes, mtDarT 8hr=Yes	Unpaired t test (Two-tailed)	NA	ns	NA	0.7319
3	E	3	empty vector 0hr=No	Spearman's correlation coefficient (ρ)	0.7239076	****	15.3586716.16232	< 2.22e-16

	E	3	mtDarT 0hr =No	Spearman's correlation coefficient (ρ)	0.4428454	****	13.54795 14.56954	< 2.22e-16
3	F	3	empty vector 8hr=No	Spearman's correlation coefficient (ρ)	0.7211051	****	15.63558 16.50517	< 2.22e-16
	F	3	mtDarT 8hr =No	Spearman's correlation coefficient (ρ)	0.4697818	****	14.17017 15.50261	< 2.22e-16
4	A	3	empty vector 0hr=No, empty vector 8hr=Yes	Unpaired t test (Two-tailed)	NA	ns	NA	0.4182
	A	3	mtDarT 0hr=Yes, mtDarT 8hr=Yes	Unpaired t test (Two-tailed)	NA	ns	NA	0.8202
4	B	3	empty vector 0hr=No, empty vector 8hr=No	Mann Whitney test (Two-tailed)	NA	ns	NA	>0.9999
	B	3	mtDarT 0hr=Yes, mtDarT 8hr=No	Mann Whitney test (Two-tailed)	NA	ns	NA	0.1
4	C	3	empty vector 0hr=No, empty vector 8hr=No	Mann Whitney test (Two-tailed)	NA	ns	NA	>0.9999
	C	3	mtDarT 0hr=Yes, mtDarT 8hr=Yes	Unpaired t test (Two-tailed)	NA	*	NA	0.0125
5	B	3	empty vector	Mann Whitney	NA	ns	NA	>0.9999

			0hr=No,empty vector 8hr=No	test (Two-tailed)				
	B	3	empty vector 0hr=Yes, empty vector 4hr=Yes	Unpaired t test (Two-tailed)	NA	ns	NA	0.3739
	B	3	empty vector 4hr=Yes, empty vector 8hr=Yes	Unpaired t test (Two-tailed)	NA	ns	NA	0.5121
	B	3	mtDarT 0hr=No, mtDarT 8hr=Yes	Unpaired t test (Two-tailed)	NA	***	NA	0.0002
	B	3	mtDarT 0hr=Yes, mtDarT 4hr=Yes	Unpaired t test (Two-tailed)	NA	ns	NA	0.0939
	B	3	mtDarT 4hr=Yes, mtDarT 8hr=Yes	Unpaired t test (Two-tailed)	NA	**	NA	0.0019
SUPPLEMENTARY FIGURES								
S1	F	3	empty vector 0hr=Yes,empty vector 4hr=Yes	Unpaired t test (Two-tailed)	NA	ns	NA	0.7035
	F	3	empty vector 4hr=Yes, empty vector 8hr=Yes	Unpaired t test (Two-tailed)	NA	ns	NA	0.5781
	F	3	empty vector 0hr=Yes, empty vector 8hr=Yes	Unpaired t test (Two-tailed)	NA	ns	NA	0.4014
	F	3	mtDarT 0hr=Yes, mtDarT 4hr=Yes	Unpaired t test (Two-tailed)	NA	ns	NA	0.436

	F	3	mtDarT 4hr=Yes, mtDarT 8hr=Yes	Unpaired t test (Two-tailed)	NA	ns	NA	0.1204
	F	3	mtDarT 0hr=Yes, mtDarT 8hr=Yes	Unpaired t test (Two-tailed)	NA	ns	NA	0.8721
	F	3	empty vector 0hr=Yes, mtDarT 0hr=Yes	Unpaired t test (Two-tailed)	NA	ns	NA	0.7024
	F	3	empty vector 8hr=Yes, mtDarT 8hr=Yes	Unpaired t test (Two-tailed)	NA	ns	NA	0.548
S2	B	3	empty vector 0hr=Yes,empty vector 8hr=Yes	Unpaired t test (Two-tailed)	NA	ns	NA	0.06
	B	3	mtDarT 0hr=Yes, mtDarT 8hr=Yes	Unpaired t test (Two-tailed)	NA	***	NA	0.0002
S3	A	3	empty vector 0hr=No	Spearman's correlation coefficient (ρ)	0.8716332	****	18.2191219.01821	<0.0001
	A	3	mtDarT 0hr=No	Spearman's correlation coefficient (ρ)	0.6697519	****	13.6442514.54359	<0.0001
	A	3	empty vector 8hr=No	Spearman's correlation coefficient (ρ)	0.8501551	****	18.4480519.30882	<0.0001
	A	3	mtDarT 8hr=No	Spearman's correlation coefficient (ρ)	0.3764233	****	11.3613712.88229	<0.0001

S3	B	3	empty vector 0hr=Yes, empty vector 8hr=No	Unpaired t test (Two-tailed)	NA	ns	NA	0.0676
	B	3	mtDarT 0hr=Yes, mtDarT 8hr=No	Unpaired t test (Two-tailed)	NA	****	NA	<0.0001
S3	C (Mip1 mNg)	3	empty vector 0hr=Yes, empty vector 4hr=Yes	Unpaired t test (Two-tailed)	NA	*	NA	0.0114
	C (Mip1 mNg)	3	empty vector 4hr=Yes, empty vector 8hr=Yes	Unpaired t test (Two-tailed)	NA	ns	NA	0.68
	C (Mip1 mNg)	3	empty vector 0hr=Yes, empty vector 8hr=Yes	Unpaired t test (Two-tailed)	NA	ns	NA	0.192
	C (Mip1 mNg)	3	mtDarT 0hr=Yes, mtDarT 4hr=Yes	Unpaired t test (Two-tailed)	NA	ns	NA	0.1832
	C (Mip1 mNg)	3	mtDarT 4hr=Yes, mtDarT 8hr=Yes	Unpaired t test (Two-tailed)	NA	ns	NA	0.4083
	C (Mip1 mNg)	3	mtDarT 0hr=Yes, mtDarT 8hr=Yes	Unpaired t test (Two-tailed)	NA	ns	NA	0.0779
	C (Mip1 mNg)	3	empty vector 0hr=Yes, mtDarT 0hr=Yes	Unpaired t test (Two-tailed)	NA	ns	NA	0.774
	C (Mip1 mNg)	3	empty vector 8hr=Yes, mtDarT 8hr=Yes	Unpaired t test (Two-tailed)	NA	ns	NA	0.5643

S3	C (*mip1*$^{e\,xo-}$ mNg)	3	empty vector 0hr=Yes, empty vector 4hr=Yes	Unpaired t test (Two-tailed)	NA	ns	NA	0.3025
	C (*mip1*$^{e\,xo-}$ mNg)	3	empty vector 4hr=Yes, empty vector 8hr=Yes	Unpaired t test (Two-tailed)	NA	ns	NA	0.8076
	C (*mip1*$^{e\,xo-}$ mNg)	3	empty vector 0hr=Yes, empty vector 8hr=Yes	Unpaired t test (Two-tailed)	NA	ns	NA	0.4644
	C (*mip1*$^{e\,xo-}$ mNg)	3	mtDarT 0hr=Yes, mtDarT 4hr=Yes	Unpaired t test (Two-tailed)	NA	ns	NA	0.8098
	C (*mip1*$^{e\,xo-}$ mNg)	3	mtDarT 4hr=Yes, mtDarT 8hr=Yes	Unpaired t test (Two-tailed)	NA	ns	NA	0.3509
	C (*mip1*$^{e\,xo-}$ mNg)	3	mtDarT 0hr=Yes, mtDarT 8hr=Yes	Unpaired t test (Two-tailed)	NA	ns	NA	0.3459
	C (*mip1*$^{e\,xo-}$ mNg)	3	empty vector 0hr=Yes, mtDarT 0hr=Yes	Unpaired t test (Two-tailed)	NA	ns	NA	0.1696
	C (*mip1*$^{e\,xo-}$ mNg)	3	empty vector 8hr=Yes, mtDarT 8hr=Yes	Unpaired t test (Two-tailed)	NA	ns	NA	0.1126
S5	A	3	empty vector 0hr=Yes, empty vector 4hr=Yes	Unpaired t test (Two-tailed)	NA	ns	NA	0.164
	A	3	empty vector 4hr=Yes, empty	Unpaired t test (Two-tailed)	NA	ns	NA	0.7354

			vector 8hr=Yes					
	A	3	empty vector 0hr=Yes, empty vector 8hr=Yes	Unpaired t test (Two-tailed)	NA	ns	NA	0.2193
	A	3	mtDarT 0hr=Yes, mtDarT 4hr=Yes	Unpaired t test (Two-tailed)	NA	ns	NA	0.278
	A	3	mtDarT 4hr=Yes, mtDarT 8hr=Yes	Unpaired t test (Two-tailed)	NA	ns	NA	0.4782
	A	3	mtDarT 0hr=Yes, mtDarT 8hr=Yes	Unpaired t test (Two-tailed)	NA	ns	NA	0.0941
	A	3	empty vector 0hr=Yes, mtDarT 0hr=Yes	Unpaired t test (Two-tailed)	NA	ns	NA	0.2656
	A	3	empty vector 8hr=Yes, mtDarT 8hr=Yes	Unpaired t test (Two-tailed)	NA	ns	NA	0.2156
S5	C	3	empty vector 0hr=Yes, empty vector 8hr=Yes	Unpaired t test (Two-tailed)	NA	ns	NA	0.6563
	C	3	empty vector 0hr=Yes, empty vector 4hr=Yes	Unpaired t test (Two-tailed)	NA	ns	NA	0.3739
	C	3	empty vector 4hr=Yes, empty vector 8hr=Yes	Unpaired t test (Two-tailed)	NA	ns	NA	0.3739
	C	3	mtDarT 0hr=Yes,	Unpaired t test	NA	ns	NA	0.7242

			mtDarT 8hr=Yes	(Two-tailed)				
	C	3	mtDarT 0hr=Yes, mtDarT 4hr=Yes	Unpaired t test (Two-tailed)	NA	ns	NA	0.9371
	C	3	mtDarT 4hr=Yes, mtDarT 8hr=Yes	Unpaired t test (Two-tailed)	NA	ns	NA	0.8315